Université d'Ottawa · University of Ottawa

Université d'Ottawa • University of Ottawa

FACULTÉ DES ÉTUDES SUPÉRIEURES ET POSTDOCTORALES

FACULTY OF GRADUATE AND POSTDOCTORAL STUDIES

Matthew L. WALLACE

AUTEUR DE LA THÈSE - AUTHOR OF THESIS

M. Sc. (Physics)

GRADE - DEGREE

Department of Physics

FACULTÉ, ÉCOLE, DÉPARTEMENT - FACULTY, SCHOOL, DEPARTMENT

TITRE DE LA THÈSE - TITLE OF THE THESIS

The Rigidity Transition in a short-chain polymer glass

B. Joos

DIRECTEUR DE LA THÈSE - THESIS SUPERVISOR

CO-DIRECTEUR DE LA THÈSE - THESIS CO-SUPERVISOR

EXAMINATEURS DE LA THÈSE - THESIS EXAMINERS

R. Carnegie

E. Fortin

M. D'Iorio

J.-M. De Koninck, Ph.D

LE DOYEN DE LA FACULTÉ DES ÉTUDES SUPÉRIEURES ET POSTDOCTORALES

DEAN OF THE FACULTY OF GRADUATE AND POSTDOCTORAL STUDIES

The rigidity transition in a short-chain polymer glass

by

Matthew L. Wallace

Thesis submitted to the
Faculty of Graduate and Postdoctoral Studies
In partial fulfillment of the requirements
For the Master of Science in Physics

Department of Physics
Faculty of Science
University of Ottawa

Your file Votre référence
ISBN: 0-494-01629-9
Our file Notre référence
ISBN: 0-494-01629-9

Abstract

In this thesis, we present a thorough investigation into the rigidity of a polymer melt above and below its glass transition (GT) at a temperature $T_G = 0.465$ (in reduced Lennard-Jones units). We use an isothermal-compression method to enter the glassy phase and NPT ensemble is realized through molecular dynamics simulations. We monitor such quantities as the mean-square displacement, the heat capacity C_P, the volume and time-dependent shear modulus $G(t)$. Whenever possible, these quantities are monitored below the GT as well. We also compute the shear modulus μ *via* external deformations and, in the zero-shear limit, find reasonably good agreement with $G(t \rightarrow \infty)$. The rigidity transition (RT) in the system is found to occur slightly *below* the GT at a temperature $T_R = 0.44$. The results are explained in terms of sufficient free volume above T_R allowing collective motion and local stress relaxation. This is seen through dynamics which are not only heterogeneous, but also spatially correlated. We appeal to notions such as "jamming" within the system and the presence of floppy modes (which allow for deformations without energy cost) to interpret the RT phenomenon. We also characterize the response to external deformation: small and large deformation regimes can be identified, the latter type causing a non-negligible reconfiguration, an over-stretching of the chains and a move to a more shallow potential energy "well." Furthermore, we analyze the "aging" phenomenon as a series of intermittent collective rearrangements and show that the two types of instantaneous shear deformations both induce "overaging," but in two completely different manners.

Sommaire

Cette thèse présente une analyse détailée de la rigidité d'un système de polymères sans solvent, au-dessus et en-dessous de la transition vitreuse (TV), qui a lieu à une temperature $T_G = 0.465$ (en unités réduites Lennard-Jones). Nous utilisons une méthode de compression isothermique pour réaliser un ensemble NPT avec des simulations de dynamique moléculaire et accéder à la phase vitreuse. Nous observons les changements dans la chaleur spécifique C_P, le volume, le déplacement moyen carré et le module de cisaillement avec dépendence sur le temps $G(t)$. Lorsque possible, les mesures sont faites des deux côtés de la TV. Le module de cisaillement μ (calculé par déformation externe) semble, à la limite d'un cisaillement nul, correspondre au $G(t \to \infty)$. Le seuil de rigidité (SR) dans notre système se trouve légèrement en-*dessous* de la TV à une temperature $T_R = 0.44$. Les résultats sont expliqués par la présence de volume libre au-dessus de T_R, permettant ainsi des grands déplacements collectifs et une relaxation du stress local. On peut observer ce phénomène à travers la dynamique hétérogène qui comprend des corrélations dans l'espace. Nous faisons aussi appel à des concepts propres à la rigidité, tels que le "jamming" du système et la présence de modes vibrationnels dits "floppy" (qui permettent des déformations sans "coût" en énergie) pour interpréter le SR. La réponse à une déformation est caractérisée par des régimes de bas et de haut cisaillement, ce dernier provoquant une réconfiguration non-négligeable et un "surétirement" des chaînes, le système se trouvant ainsi dans un puits de potential moins profond. Par ailleurs, nous analysons le phénomène de "vieillissement" comme étant une série de réarrangements collectifs et intermittents dans le système. Nous montrons que les grands et petits cisaillements instantanées induisent un "survieillisement", mais de deux façons bien différentes.

Acknowledgements

I would like to thank my supervisor Dr. Béla Joós for excellent guidance and support throughout my M.Sc. programme. I would also like to acknowledge Dr. Mike Plischke of Simon Fraser University for providing useful insight, as well as elements of the source code used in the simulations. Finally, thanks to my colleagues in the department for their help, enlightening discussions and overall good times during the past years.

Contents

List of Figures

List of Tables

Chapter 1 Introduction

The focus of the present thesis is on the behaviour of a polymer melt – a typical "fragile" glass former – as it becomes rigid. As a polymer melt is cooled, the dynamics slow down. In fact, this slowing-down is so powerful that eventually, the liquid appears to fall out of equilibrium on a given timescale and forms a glass. While this process is fairly well-understood, two important questions remain: 1) At what temperature does the rigidity occur? and 2) What makes the system rigid? The interest of the present work is that we are investigating a new *kind* of rigidity: one which does not rely on physical constraints and one which may be strongly timescale-dependent. Furthermore, we would like to characterize the rigidity of the glass by seeing how it responds to external deformations. As we will show, these responses are fairly complex.

1.1 Investigating rigidity

From a purely mechanical standpoint, there are obvious benefits to understanding the origins of rigidity. While a coherent theory for describing generic rigid systems is only recent (see Ref. [1] for a complete review), the applications of this field go beyond an understanding of what makes a structure rigid. A recent novel application to rigidity theory deals with the problem of protein folding as an example of a rigid to flexible transition, using an approach similar to the analysis of network glasses [2]. In general, however, the field of rigidity is restricted to a very small number of researchers, and most of the work done relates to very specific materials, such as network glasses. The tools developed in the context of rigidity theory, however, could have a more general use. As an example, we refer to the recent discoveries showing

how the way in which rigidity "spreads" within a system can ultimately determine what kind of solid will be produced [3, 4].

1.2 Polymers, glasses and soft condensed matter

Over the past few decades, materials such as polymers and colloidal suspensions have been made to form glasses, gels, foams, plastics and other "soft matter" with desirable mechanical properties. Some of these seemingly bizarre properties, such as shear thinning, aging and generally non-Newtonian behaviour are only recently beginning to emerge. The mechanical properties of soft matter materials give them a wide range of applicability: from high-elasticity rubbers to colloidal suspensions used in food processing to plastics obtained from polymer glasses. However, we have only recently begun to understand the physical origin of these properties.

In recent years, many advances have been made towards the understanding of the glass transition (GT) (see Refs. [5, 6, 7] for a good review). Supported by a wealth of experimental data, many theoretical models now exist to explain the origins of kinetic arrest, although a *complete* theoretical model explaining the observed properties of the GT is still lacking. For instance, while the physics behind elastic properties arising from crystallization is well-understood, the same cannot be said for glasses in general.

1.3 What makes a glass "solid"?

From a purely geometric point of view, the problem of rigidity is no longer a mystery. A mean-field approach based on degrees of freedom and constraint counting has been very successful in understanding rigidity in glasses containing many chemical bonds [1]. Without constraints, we must appeal to different direct and indirect methods of observing rigidity. This could mean applying external forces or, on another level, examining macroscopic quantities such as viscosity and overall stress in the system as well as thermodynamic quantities such as the heat capacity C_V. The latter, for

example, is crucial because it can provide information on the number of configurations or modes available to the system. We would also like to examine the *microscopic* origins of this rigidity since, ultimately, stress remains present in a deformed, rigid system due to its inability to reorganize locally.

As we will see, we are also faced with the problem of investigating a material which is, by definition, out of equilibrium. Although very slow, the evolution in time (called "aging") of a glass will also affect its rigidity.

1.4 Organization of the thesis

We will begin in Chapter 2 by giving a review of the relevant work done both in fields relating to rigidity theory and those relating to the glass transition. We also include some relevant information relating to polymers in general. An emphasis will be put on useful theoretical models which successfully explain experimental results, as well as recent computer simulations which have provided additional insight into the supercooled or glassy state. The equations cited or derived in this chapter will prove useful in our calculations. In Chapter 3, we provide details on how the system was modelled, techniques for simulating the dynamics and explicit information relating to how the calculations were performed. In Chapter 4, we will present the results obtained from the simulations, organized in a way to give a semi-complete characterization of the GT and glassy state of the polymer system with particular emphasis placed on the rigidity transition. The results presented will be accompanied by brief explanations as to their significance. A relatively short, but more in-depth discussion in Chapter 5 will analyze the results within the current theoretical framework of glasses and rigidity. We will attempt to elucidate some of the mechanical properties of a fragile polymeric glass with respect to local behaviour and general "aging" phenomena. Finally, Chapter 6 will conclude with a summary of the most crucial results and provide a general outlook on future research in this field. To facilitate the reading, a list of the main symbols and acronyms used can be found in Appendix B.

Many parts of this thesis are taken from an article which has been published in the journal *Physical Review E* in October 2004 [8]. These results have also been presented at several conferences of the American Physical Society and of the Canadian Association of Physicists. Data and discussion pertaining to the aging process, heterogeneous dynamics and rejuvenation/overaging have not yet been submitted for publication.

Chapter 2 Theory

2.1 The Rigidity Transition

We can define a rigid structure as one that displays some resistance to shear (a non-zero shear modulus μ) and a divergence in viscosity η. In other words, a non-zero μ implies an inability to deform without a cost in energy. The shear modulus is defined as

$$\mu = \frac{\sigma_{\alpha\beta}}{\epsilon_{\alpha\beta}}, \quad \alpha \neq \beta \tag{2.1}$$

i.e. the stress response to a given (imposed) off-diagonal strain. Similarly, we can define a time-dependent shear modulus $G(t)$, which measures the response of the system to a shear strain $\epsilon_{\alpha\beta}$ applied at $t = 0$ as [9]

$$G(t) = \frac{\sigma_{\alpha\beta}(t)}{\epsilon_{\alpha\beta}}, \quad \alpha \neq \beta \tag{2.2}$$

where $\sigma_{\alpha\beta}$ is an off-diagonal macroscopic stress tensor element. Clearly, $G(t)$ and μ should be identical in the long-time limit, although, as we shall see, the calculation methods for the two quantities are generally different. To our knowledge, the equivalence has never been checked explicitly. Given that, by definition, $G(t)$ or μ defines the stress response to an arbitrary shear strain (*i.e.* a "modulus" in its general sense), we can isolate $\sigma_{\alpha\beta}$ in Eq. (2.2) and express it as a stress response based on a sum of previous relaxations

$$\sigma_{\alpha\beta} = \int_{t'=-\infty}^{t} G(t-t')d\epsilon_{\alpha\beta}(t') \tag{2.3}$$

which is simply an application of the Boltzmann superposition principle and is valid because the stress response depends solely on earlier relaxations [9]. Substituting

$d\epsilon_{\alpha\beta}$ by $\dot{\epsilon}_{\alpha\beta}dt$ (assuming the strain is applied in a constant manner), and making a change of variables $t'' = t - t'$, we obtain

$$\sigma_{\alpha\beta} = \dot{\epsilon}_{\alpha\beta} \int_{t''=0}^{\infty} G(t'')dt'' \tag{2.4}$$

This equation can be combined with the basic equation of Newtonian liquids, postulated as

$$\sigma_{\alpha\beta} = \eta\dot{\epsilon}_{\alpha\beta} \tag{2.5}$$

where η is the zero-shear viscosity. It should be noted that we make use of this equation in the low shear-rate limit, which is sufficient for local fluctuations. For non-negligible shear rates, the viscosity can display non-Newtonian behaviour. Combining Eqs. (2.4) and (2.5) yields

$$\eta = \int_{0}^{\infty} G(t)dt, \tag{2.6}$$

meaning that a diverging viscosity and non-zero shear modulus are equivalent.

At a non-zero temperature, entropic rigidity occurs at the onset of connectivity percolation, *i.e.* when two sides of a given system are connected [10, 11, 12]. Entropic rigidity arises from a system attempting to return to a high-entropy state and therefore is especially dominant in many highly entropic systems, such as cross-linked polymer melts [11] and diluted central force networks [10]. Mechanical rigidity, which is purely energetic, is the most widely studied form in the case of network glasses, such as SiO_2. A common method for interpreting this is by looking at the number of "floppy modes" in the system. In this context, floppy modes are zero-frequency modes which can allow deformations without cost in energy at $T = 0$ [13]. This begs the question: what determines whether there are floppy modes present? These modes will arise from the degrees of freedom present in each particle that composes the system. From a mean-field approach, the number of floppy modes f will tend to zero when the number of constraints reaches the number of degrees of freedom. In a bond-bending network, for example, it has been found that a mean coordination

number $\langle r \rangle$ (the average number of bonds per particle) equal to 2.4 corresponds to the onset of mechanical rigidity [3, 13]. This concept has proven useful in understanding the formation of network glasses [3, 4, 14, 15, 16], which are "strong" as opposed to "fragile" polymeric glasses. The distinction between the two types is explained in Section 2.4.1.

From a macroscopic point of view, mechanical rigidity requires a percolating rigid backbone, and thus requires more bonds than for simple connectivity. In a system where the forces are entirely due to pair interactions, rigidity often begins with the increase in size of rigid clusters, leading to the formation of a gel. In fact, the particular type of structure that forms is thus determined by how the rigidity organizes locally [3, 4, 13]. Specifically, if a system is over-constrained, then local rigidity will be allowed to "nucleate" and crystallization can occur. If such a situation is prevented, then we will observe a general "jammed' state and a possible GT. The mechanism responsible for this has been called "self-organization," meaning that the system can form local defects to avoid stress (over-constraints). This self-organization, however, is subtle and unlikely to be resolved by diffraction experiments [3]. Rigidity in strong glasses is directly related to the network of covalent bonds that forms, making constraint counting an ideal way to study them. Glasses can also be formed by "jamming," which effectively takes the place of the chemical connections. Recent research suggests that rigidity in gels and glasses are due to the same phenomenon: the jamming induces a kinetic rather than thermodynamic onset of rigidity [17, 18]. It has been found that jamming leads to critical-like behaviour of both the viscosity and shear modulus around critical points determined by the density or temperature.

Most previous studies of the rigidity transition are percolation-based, more suitable for the appearance of rigidity due to gelation (known as the sol-gel transition). Consider a branched polymer, for instance, which is able to make multiple connections and form an increasingly large tree-like structure [19]. As its size increases, the (liquid) system will become more and more viscous until the cluster percolates across the system. It has been found that, in this case, both the viscosity and the shear modulus show power-law behaviour, based on the distance to the percolation point

$p - p_c$. One can define p, for example, as the degree of connectivity in a branched system [19]. The creation of an infinite cluster (in the thermodynamic limit) causes a divergence in the length scale ξ of the system. Gelation can be observed in simulation simply by cross-linking short polymer chains, producing the desired divergence in viscosity and appearance of the shear modulus at the percolation point [20, 21].

2.2 Polymer structure and dynamics

Polymers are a broad category of materials, and understanding their properties has proven very useful not only in fields such as biochemistry, but also in materials science. In our context, the primary function of the polymer model is to facilitate the formation of a glass. However, the model also has important physical significance, as will be discussed in detail in Section 3.1. For this reason, it is worthwhile to very briefly review some basic polymer properties. The viscoelastic properties of cross-linked and natural rubber, for instance, have made it a substance with thousands of practical applications. Polymer chains can assume many different shapes, such as branched, star-shaped and linear polymers. We will restrict our discussion to the latter type, with identical repeat units.

Furthermore, we will restrict ourselves to the behaviour of bulk polymer melts, *i.e.* three-dimensional materials where there is no solvent present. The static properties of a given chain are best described by its mean squared radius of gyration or end-to-end distance, defined by

$$R_G^2 = \left\langle \frac{1}{M} \sum_{i=1}^{M} |\mathbf{r}_i - \mathbf{r}_{CM}|^2 \right\rangle \tag{2.7}$$

$$R_{EE}^2 = \langle |\mathbf{r}_1 - \mathbf{r}_M|^2 \rangle \tag{2.8}$$

where $\mathbf{r}_j$ is the position of a given monomer, $\mathbf{r}_{CM}$ is the position of the centre of mass of the chain, M is the number of elements on a chain and $\langle \cdot \rangle$ represents an average over all chains in the system. The radius of gyration can also be used to

describe the shape of any generic cluster (not necessarily formed by a chain) [22]. The shape of the chain approximately follows a self-avoiding random walk and ideal chains obey the characteristic ratio $R_G^2/R_{EE}^2 = 6$ [23], which we were able to check in our system. The shape is therefore (up to certain point) independent of the length of a polymer. When it comes to the dynamic properties of a melt, the same is not true. For relatively short (or low molecular weight) chains, we can describe the dynamics fairly well using the Rouse model. Briefly, the Rouse model was first applied to dilute polymer solutions. The underlying assumptions are that the chains are composed of a series of particles under going Brownian motion and connected by harmonic springs [9, 24]. The Brownian motion leads to the assumption of a uniform local friction coefficient acting on all particles [25]. A given chain is then divided into M "Rouse" segments and the springs, combined with the friction force, leads to a differential form of the equation of motion for a given monomer (see Refs. [9, 24] for more details). The Rouse model is able to correctly predict properties such as the viscosity η and the diffusion constant D in the liquid regime, which are proportional to M and M^{-1} respectively [23].

When dealing with longer chains (as is the case for the most commonly-known polymers), the chains can become entangled, forming something analogous to a knot between two chains or between two distant points on a single chain. Longer chains move by reptation, since they must "snake" through the network of entanglements. Although the simulation of very long chains would be desirable, we will restrict ourselves to the dynamics of short, non-entangled chains.

Upon cooling, polymers display a wide range of phenomena. Certain types of polymers have been seen to form crystalline or partially crystalline structures by organizing themselves into lamellar structures, for instance [9]. However, due to the complex, disordered shape of most polymer melts or solutions, rearrangement into ordered structures is difficult, and practically impossible when there is no *a priori* orientational order within the chains, as in the case of our simulations. For this reason, many polymers tend to form amorphous structures upon cooling, with no long-range order. As will be discussed in Section 3.1, the structure of the polymer

makes it susceptible to be geometrically frustrated before it can even begin to acquire any type of order. It therefore undergoes a transition to the glassy state.

2.3 The Glass Transition

2.3.1 Signatures of the GT

In a purely liquid short-polymer melt, the Rouse model has been able to quantitatively explain most of the dynamics of the system [9, 24]. When the system is cooled towards glassy state, there can be a very large increase in viscosity η or relaxation times τ. The Rouse model can account for this type of behaviour as an increase in the friction coefficient mentioned in the previous section, and can account for many polymer properties in the supercooled regime [25]. However, new interpretations are also required to fully explain the dramatic slowing-down of the system. Thus, in order to understand the behaviour from a more rigourous perspective, we must appeal to the notion of a glass transition (GT).

Upon cooling, a liquid may crystallize, but if it fails to do so, we say that the liquid is supercooled. Further cooling will inevitably lead to the formation of a glass. The crystallization is generally avoided by a fast cooling rate. Most of the glass-forming liquids studied (such as ours) have difficulty crystallizing (because of competing length scales, for instance), so we may cool them at a relatively slow rate. The GT is not yet a completely well-understood phenomenon and can be most simply described as a "structural arrest" [5, 6, 7]. As a liquid is cooled, it is constantly re-arranging its configuration in order to maintain thermodynamic equilibrium. This can be done because there is enough free energy available to the system. However, as the temperature is lowered there comes a point (known as T_G, the GT temperature) when the system cannot reconfigure on the timescales of the experiment and becomes "trapped" in a non-equilibrium state for a relatively long time. As such, the glassy state ($T < T_G$) is in a non-equilibrium state, because it ages over time, as will be discussed further on. This means that the temperature T_G will be highly dependent on the cooling rate: a faster cooling rate causes the system to be trapped at a higher

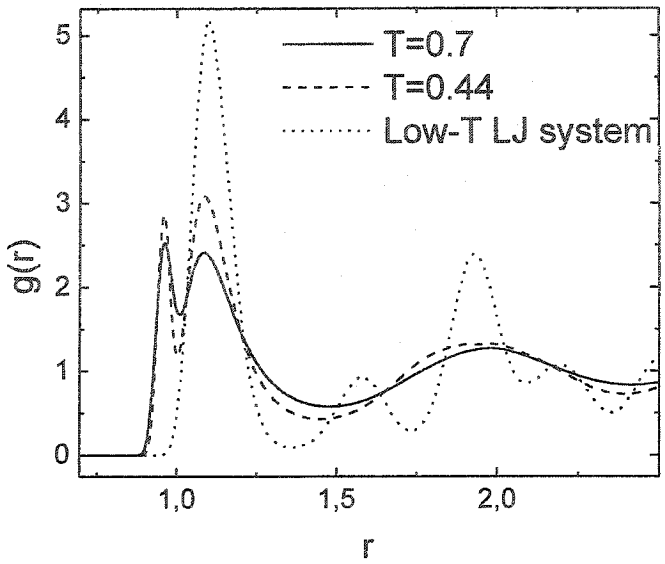

Figure 2.1: The radial distribution function for a polymer melt in the glassy and liquid phases, as well as a pure LJ system. While both polymer melt curves show liquid structure, the additional peaks for the LJ system indicate the presence of crystalline regions. Note the two initial peaks for the melt corresponding to the LJ and FENE potentials discussed in Section 3.1.

temperature [26]. The difference between crystal and glass formation is best seen *via* the radial distribution function (RDF), which, assuming structural homogeneity, can be computed as [27]

$$g(r) = \frac{V}{N^2} \sum_{i=1}^{N} \sum_{j=1}^{N} \delta(\mathbf{r} - [\mathbf{r}_i - \mathbf{r}_j]), \quad i \neq j \tag{2.9}$$

where V is the volume, N the number of particles and δ the Delta-Dirac function for differences in particle positions $\mathbf{r}$. Typical liquid, glassy and crystalline RDFs are shown in Fig. 2.1.

The GT is characterized by an increase in relaxation time τ of many orders of magnitude. The viscosity η and the relaxation time can be related through the expression

$$\tau = \frac{\eta}{G_\infty} \tag{2.10}$$

where G_∞ is the infinite-frequency shear modulus, which has relatively little temperature dependence. Experimentally, T_G is defined as the temperature when the viscosity reaches 10^{12} Pa·s. This is a "practical" definition, as this high viscosity value implies that there is little motion on ordinary experimental timescales. As such, the GT is not actually a transition in the thermodynamic sense (*i.e.* with discontinuities in thermodynamic properties). However, there is seen to be a large change in functions such as the heat capacity and expansivity, so we may consider the GT to be a "pseudo second-order transition," since the discontinuities are not sharp and occur over a range of temperatures [28].

A manifestation of this transition is a change in the constant pressure heat capacity C_P, defined as

$$C_P = \frac{1}{N}\left(\frac{\partial H}{\partial T}\right)_{N,P}, \tag{2.11}$$

where $H = E + PV$ is the enthalpy. While there is no discontinuity, the heat capacity is generally seen to undergo a small increase followed by a large decrease upon cooling through T_G.

The glass transition is also marked by a change in the thermal expansivity $(\frac{\partial V}{\partial T})_P$ [28]. Since the glass can no longer reconfigure, the volume cannot respond to a change in temperature on the timescale of the experiment or simulation.

In order to gain further insight into the GT, a multitude of models exist to explain how liquids behave as they are cooled without crystallizing. As the number of different models is quite large and they take many different approaches, we will restrict our discussion to those which are most widely accepted and have the most relevance to our observations. The reader is referred to Refs. [5, 6] for a complete review.

2.3.2 Free volume

One of the first explanations for glassy behaviour is based on a free volume approach. Today, the theory still evokes some interest, albeit primarily only on a qualitative level. The main concept behind it is that the local rearrangements depend on the amount of local free volume. Specifically, transport phenomena are determined by the probability to find local free volume exceeding a critical value [29]. Although this approach is able to reproduce several of the empirical formulae (such as VFT, explained below), the approach is by no means rigourous and the reader is referred to [29] for a concise review. Nevertheless, the concept of free volume will prove to be useful in understanding the behaviour in glasses, especially with respect to relaxation. One interpretation predicts a transition point where there is no longer any free volume present in the system [28]. It has been verified that this point is *not* T_G, and such a point may not be accessible, as we shall see later, but may remain useful in characterizing a material. For example, a recent scaling approach by Colby (discussed below) relies on the presence of mobile areas of free volume to explain the presence of a critical point T_C below T_G [30].

2.3.3 Mode-coupling theory

Mode-coupling theory (MCT) provides one of the few complete theoretical frameworks for the GT in simple liquids. It is an approach based on a microscopic description of dynamics and fluctuations within a supercooled liquid [29, 31]. Essentially, an MCT (in general) states that the fluctuation of a dynamic variable decays into pairs of hydrodynamic modes [32]. It has been found that supercooled liquids are dominated by two types of relaxation processes: α-relaxation, which is slow (low-frequency) and β-relaxation, which is fast (high-frequency). Idealized MCT (which does not allow for any type of "barrier hopping" or activated processes) predicts that at some $T_{MC} > T_G$, there will be a decoupling of the relaxation modes and a loss of ergodicity in the system. This idealized version predicts that the viscosity scales as

$$\eta \sim (T - T_{MC})^{-s}. \tag{2.12}$$

The divergence at T_{MC} is generally not observed, most likely due to the appearance of thermal activation effects, allowing a local configuration to change by overcoming a large free energy barrier [29, 33]. New "extended" MCT approaches allow for such processes with the addition of an *ad hoc* parameter, but there is no concrete evidence that MCT can explain the behaviour in the range $T_G < T < T_{MC}$.

2.3.4 Entropy and the VFT equation

The third approach we will discuss is entropy-based. The passage from the liquid to crystal state is characterized by a large drop in entropy, since the number of states accessible to the system becomes very small. The relevant part of this entropy is called configurational, meaning that for a high configurational entropy system, very few particles need be involved in a rearrangement to an equivalent state. When the configurational entropy is low, the opposite is true. We can associate an ideal "crystal-like" glass to a zero configurational entropy, characteristic of a second-order transition at the Kauzmann temperature T_K [28]. This state, however, is never reached, due to the slow dynamics (high viscosity) of the system. The interest of the Kauzmann temperature is that below it, the entropy should theoretically become negative, so to prevent this the GT should be some type of manifestation of a second-order phase transition at T_K. The theory was first developed by Adam and Gibbs, who were able to relate the viscosity to the configurational entropy S_C as [34]

$$\eta = A \exp\left(\frac{B}{TS_C}\right) \tag{2.13}$$

where A and B are constants. This indicates that there should be a divergence in viscosity at the hypothetical $S_C = 0$ point [28]. A recent development has been able to relate the configurational entropy to spatially correlated, heterogeneous dynamics, which are crucial to the relaxations on approaching and below T_G, as will be discussed in detail in Section 2.4.4. Specifically, it has been found that the size of the clusters of

mobile particles is inversely proportional to the configurational entropy of the system [35].

The most successful and useful analysis of glass-forming liquid dynamics is empirical and has been observed for many decades. It is now known as the Vogel-Fulcher-Tammann (VFT) equation, which we can express in terms of viscosity as

$$\eta = \eta_\infty \exp\left(\frac{E_{act}}{T - T_0}\right) \tag{2.14}$$

where E_{act} is an activation energy and η_∞ is the viscosity at infinite temperature. T_0 can be calculated by a fit to Eq. (2.14), while T_K can be extrapolated by calorimetric measurements. Experimental results indicate that these temperatures are identical or very close, and therefore represent the same phenomenon [6, 28]. We can therefore associate the configurational entropy with T_0 by the following relation

$$S_C = \int_{T_0}^{T} \Delta C_P d(\ln T) \tag{2.15}$$

where ΔC_P is the T-dependent difference in heat capacity between the liquid and ideal glass state at T_0, which is approximately that of a crystalline state [7, 28, 34]. Given that there is experimental evidence for $C_P \sim 1/T$, the integral yields

$$S_C = a\left(\frac{T - T_0}{T T_0}\right) \tag{2.16}$$

where a is an integration constant. Substituting this result into Eq. (2.13), gives the empirical VFT relation of Eq. (2.14). So, by a somewhat *ad hoc* method, one is able to gain some insight into the origins of viscosity (or relaxation time) behaviour across the GT. To make a connection with rigidity, it has also been proposed that (in general) at T_G, the fraction of floppy modes f becomes sufficiently small for the system to freeze on the timescale associated with a given cooling rate, while f should tend to zero on approaching T_0 [36].

2.3.5 Dynamical scaling approach

Similar to the percolation-based ideas, a dynamical scaling approach was recently proposed to explain the extrapolated divergence in relaxation below the GT [30]. The approach relies on free volume and dynamical heterogeneity, as will be discussed in more detail in the following section. It is claimed that between a critical temperature T_C and the glass transition temperature T_G, there is sufficient free volume for limited motion to occur. Just as in the case of percolation, we can construct an order parameter which is defined as the fraction of space with sufficient free volume. From this basis, universal behavior among glass-forming liquids is assumed and the viscosity is seen to diverge as

$$\eta \sim \left(\frac{T - T_C}{T_C}\right)^{-9} \exp\left(\frac{E}{k_B T}\right) \tag{2.17}$$

where the first term should suffice for very fragile glasses and the second term describes the additional Arrhenius-type activation energy to ensure universality for *all* glass formers. Unlike the MCT approach, the above equation yields a critical temperature for viscosity divergence T_C below T_G. Comparison with experimental data was seen to be very accurate [30]. The advantage of this approach is that the scaling argument derives from a basis similar to that of a sol-gel transition, for instance. However, we are once again faced with the problem of how to probe temperatures below T_G.

2.3.6 Energy landscapes

A very useful perspective for gaining insight into the dynamics of glasses is by considering an energy landscape, which is essentially the potential energy function determined by $\mathcal{O}(\mathrm{N})$ coordinates, the precise value depending on the degrees of freedom of the particles [6, 7]. We then have a picture of a hypersurface punctuated by local minima of varying depth, and an overall shape determined by volume (assuming constant N). The *sampling* is thus determined by the temperature of the system. Unlike a crystal, which would have one dominant minimum, a glass has many. In the

context, we can define the state at T_G as being stuck in one of these fairly deep local minima and the hypothetical ideal glass state as a global minimum. While explicit calculations can reveal both the shape and the sampling of the landscape, we appeal to the energy landscape as a qualitative guide to the observed glassy phenomena. As we shall see, the complexity of energy landscapes in glasses makes this concept very useful.

2.3.7 *Previous simulations of glassy polymers*

Previous simulation work regarding the glass transition in (fragile) glass-forming polymers has been mostly done by the group of K. Binder *et al.* [25, 26, 29, 37, 38, 39]. Their work has focused on the behaviour of the supercooled melt as the GT is approached. They have studied α and β relaxation modes, cooling-rate dependencies, the applicability of MCT, the relation with Rouse modes and the dominance of the cage effect. Their studies have been done using both molecular dynamics and Monte-Carlo computer simulations.

2.4 The glassy state

2.4.1 *Fragility*

Glasses can often be distinguished in terms of their fragility. We must point out that the rigourous definition of "fragility" in a glass has nothing to do with what is commonly thought of as being brittle; it is a somewhat more subtle concept. The most obvious definition of fragility relates to the energy landscape of a glass, in that the landscape of a fragile glass will be punctuated by a larger number of local minima than that of a strong glass [6, 7]. This means that fragile glasses will be able to visit more configurational states. In fact, the fragility of a glass can be found by examining the viscosity increase on approaching T_G from above. If the increase in viscosity is characterized by Arrhenius-like behaviour (as in the case of strong glasses), then the activation energy is constant [7], *i.e.*

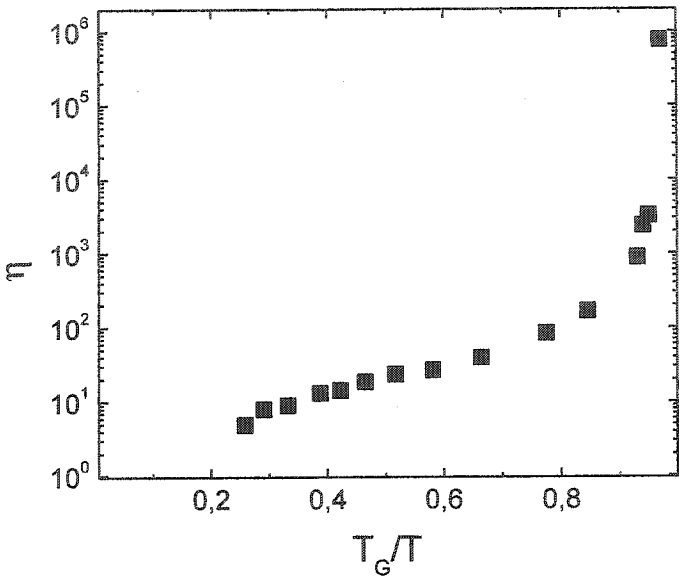

Figure 2.2: Glassy behavior of the polymer melt shown in a typical Arrhenius plot. The large slope close to T_G indicates that the glass is primarily fragile.

$$E = \frac{\mathrm{d}(\ln \eta)}{\mathrm{d}(1/T)} \approx \text{const} \tag{2.18}$$

Fragile liquids, however, exhibit super-Arrhenius behaviour as the activation energy increases with temperature. Fig. 2.2 shows our data, which clearly displays fragile behaviour on approaching T_G. Similarly, one can define an index of fragility m, equal to the slope of Fig. 2.2 at T_G [40]. Strong glass formers, such as SiO_2, are often structurally more stable due to the presence of strong bonds, as opposed to weak van der Waals bonds. If a glass is formed primarily due to geometric frustration, then it is considered fragile. For this reason, computer simulations of fragile glasses generally use polymers, as in the present case, or binary Lennard-Jones liquids. The latter is a mixture of Lennard-Jones spheres with two different potentials, yielding two incompatible length scales.

2.4.2 Gels vs. glasses

While the formation gels is associated with a diverging length scale due to the increase in cluster size, glasses are not known to have a dynamic length scale at all. In other words, they are structurally homogenous. This can be most easily seen in the structure factor $S(\mathbf{q})$, which can be found by scattering experiments or extracted from a Fourier transform in a simulation as

$$S(\mathbf{q}) = \sum_{i=1}^{N} \sum_{j=1}^{N} \exp[i\mathbf{q}\cdot(\mathbf{r}_i - \mathbf{r}_j)] \tag{2.19}$$

where $\Delta\mathbf{r}$ represents a particle displacement and $\mathbf{q}$ is a wavevector representing the reciprocal lattice.

$S(\mathbf{q})$ does not qualitatively change much when passing from the liquid to glassy phase. In gels, however, a peak around $\mathbf{q} = \mathbf{0}$ can develop, due to increase in characteristic length scale. Fig. 2.3 shows the structure factor in the glassy and liquid phases for our model. One advantage of this property of glasses is that simulations can be done without being overly concerned with finite-size effects, while simulations near the gel point are very sensitive to system size, and finite-size scaling arguments must often be used [21]. Gels, however, do not always display the same ergodicity-breaking as glasses, which are unable to access their potentially large phase space due to the slow dynamics.

Despite these differences, it has been suggested that certain gels and glasses can be characterized as "fragile soft matter" or "jammed" states [41, 42, 43]. A jammed system is essentially stuck in a small region of phase space and local re-arrangement is greatly hindered. While many such materials can be formed by imposing external constraints, a jammed state can occur naturally if the temperature is low enough and, more importantly, if the density is very high. The "solid" nature of a glass is primarily due to caging. The cage effect is a signature of a GT and occurs when the nearest neighbours of a particle become so close that the particle's movement becomes greatly restricted, since it can no longer escape easily by going in between two neighbours. This effect is amplified in the case of polymers, where the chain

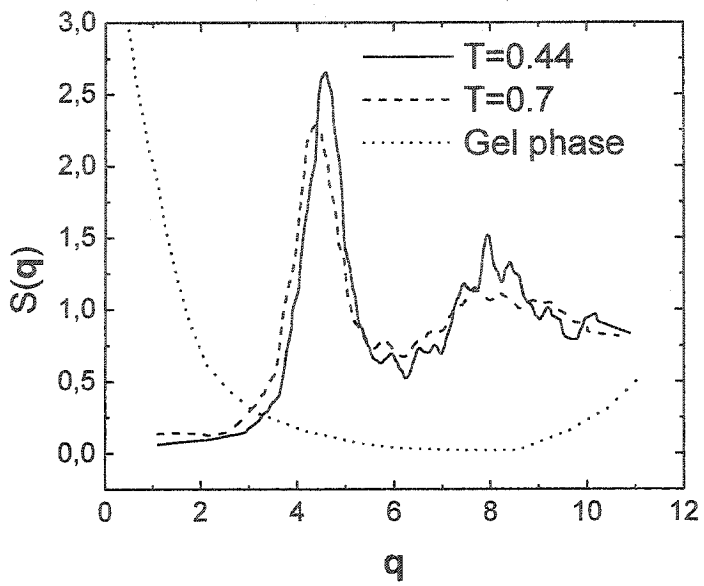

Figure 2.3: The calculated structure factor $S(\mathbf{q})$ of a glassy (T=0.44) and liquid (T=0.7) polymer system. Note that both have similar shapes and that the first peak corresponds to the approximate nearest-neighbour distance. An approximate sketch of $S(\mathbf{q})$ for possible gel-like behaviour is also included. The emergence of a peak at higher wavevectors is for the case where the particles "stick" together at smaller distances. The behaviour at small q indicates a diverging length scale.

connectivity means that even if a given monomer can barely escape, it is quickly pulled back by it's neighbours along the chain [25].

2.4.3 *Aging, rejuvenation and overaging*

The glassy state is characterized by a non-equilibrium system which evolves on very large timescales, due to the slow dynamics. If we characterize a glass by a system with excess entropy (with respect to a hypothetical ground state, such as a crystal) the process whereby the "trapped" system loses its excess entropy is known as aging. We can interpret this as the system hopping to lower local minima in its energy landscape over a long period of time. Normally, one would therefore observe a slow energy decrease and a general slowing-down of the dynamics. Aging phenomena can be observed both experimentally and by simulation, provided the timescale of

the relaxations is very slow. If a system is quenched instantaneously from a high temperature (say T_A) with short relaxation times to a low one (say T_B) with very long relaxation times, then the system will attempt to reconfigure itself to a state corresponding to T_B. Initially, fast relaxations (within the cages) will be quick, but slow α-relaxations (re-arrangement of the cages or "escapes") will take much longer and depend on the waiting time t_w [44]. Intuitively, this seems reasonable: re-arranging the cages themselves requires cooperative motions, which is difficult in such a slow system. The aging phenomenon can be seen through the time-dependence of ordinary quantities such as the potential energy, as the system slowly moves to lower potential wells in its energy landscape. These quantities are called "one-time" since they depend only on the time elapsed since the quench. In fact, it has been found that this dependence is quite weak [45, 46]. Experimentally, one typically measures the evolution of response functions, such as the elastic compliance, over large timescales (*e.g.* days) to observe aging [46]. An important consequence of aging is that, as the system is slowly losing some of its excess entropy, the dynamics will become slower.

A more useful approach, especially for simulations which can only access a limited range of time, is to measure "two-time" correlation functions, which depend on a time τ (as is the case for any time correlation) and on the time since the quench t_w. These functions are useful because they are representative of the separated timescales of the fast and slow relaxations in the aging regime. We can therefore generalize the "self" part of an incoherent scattering function to this non-equilibrium situation as [45]

$$C_{\mathbf{q}}(t_w+\tau,t_w)=\frac{1}{N}\sum_{j=1}^{N}\exp[i\mathbf{q}\cdot(\mathbf{r}_j(t_w+\tau)-\mathbf{r}_j(t_w))] \tag{2.20}$$

where $\mathbf{q}$ represents a given wavevector in the reciprocal lattice. This function essentially measures how long it takes (τ) for a particle to "forget" an earlier position. This type of calculation has been extensively used in simulations of glassy Lennard-Jones systems and it has been found that for longer waiting times, it takes longer for a system to forget its initial configuration [45, 46]. We have obtained similar results, yielding a typical decay curve for our system, seen in Fig. 2.4. It is thus possible to determine the effect of initial and final temperatures, as well as waiting

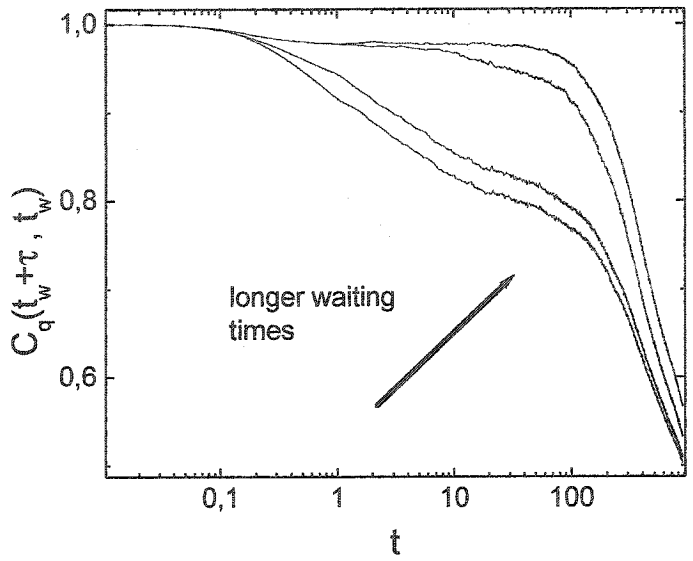

Figure 2.4: The two-time scattering function of Eq. (2.20) at different waiting times t_w. In the direction of the arrow, $t_w = 0, 10^2, 10^4, 5 \times 10^5$. After a instantaneous quench from T=1.8 to T=0.275, the dynamics become slower as the system ages.

times. While Fig. 2.4 appears to show continuous decay, this is simply a consequence of averaging over many samples: each individual sample shows that the large decorrelation characteristic of α-relaxation is step-like and occurs *via* "catastrophic" events. These events correspond to momentary collective dynamical motion (see next section), which significantly changes the local stress [46].

There are many models to explain aging in glassy systems and the reader is referred to Refs. [44, 47] for a complete review. One of the most interesting aspects of aging can be seen upon imposition of a large external driving force such as shear flow, which can have the effect of "rejuvenation." By this we mean that the memory of the system is wiped out and the dynamics become faster, in contrast with the normal aging process. This is related to the "shear thinning" phenomenon, where the viscosity is reduced during the application of a continuous high-shear driving force [48]. The most useful interpretation of this is known as the "trap" model first proposed by Bouchaud [49] and the related "soft glassy rheology" (SGR) model to

explain the effect of shear [50]. In the glassy state, the system evolves slowly in the energy landscape, as discussed earlier. Knowing how the minima are distributed, one can also know, at a given temperature, at what rate the system is able to escape from these minima. Given a local minimum of depth E, we can associate a local strain l, giving rise to a local stress kl, where k is an elastic constant. At a given yield strain l_y, the particles rearrange to new positions, allowing stress relaxation. More generally, the larger the strain, the more likely a particle is able to escape from its "trap." If we can consider a glass as a jammed system, just as in the case of a foam or a pile of sand, then the system can be "unjammed" by applying a stress or deformation. This can be most easily seen for the case of a pile of sand, where tapping it slightly causes it to rearrange and forget its earlier configuration [41].

Recently, however, Viasnoff *et al.* have observed that one can "overage" a colloidal glass after imposing a *transient* shear perturbation [51]. Applying shear changes the distribution of relaxation times, and can yield many different responses. Considering that the system has a wide distribution of α-relaxation times with their own characteristic energies, overaging effectively means overpopulating the long relaxation times (compared to a "reference case"), yielding slower dynamics. Rejuvenation, on the other hand, corresponds to the overpopulation of short relaxation times. These effects can both occur simultaneously, but with different timescale-dependencies, *i.e.* one must once again look at various waiting times t_w. One can also observe the same type of phenomenon after imposing a small temperature perturbation [51]. It has been found that, within the context of the SGR model, overaging will eventually occur after any finite shear perturbation, but cannot occur *during* the application of steady shear.

2.4.4 Dynamical heterogeneity

While a glass does not display the same heterogeneous structure as a gel, the same cannot be said for its dynamics. The presence of dynamic heterogeneities in glass-forming liquids has therefore been thoroughly investigated [52, 53]. In looking at

the system as a whole, one can simply monitor the mean-square displacement (MSD) $\langle \Delta \mathbf{r}^2(t) \rangle$ based on some initial reference positions, where we are averaging over all the particles. Initially, the particles move freely with a constant velocity and therefore the MSD should have a t^2 dependence. Once the collisions begin to occur, the MSD will evolve more slowly. Eventually, if the particles are localized on long timescales, the MSD will reach a plateau. However, if diffusive behaviour is possible, then the MSD will become linear with time.

Above but near the GT, it has been found that polymer melts can also display sub-diffusive behaviour, where the MSD of the monomers goes as approximately $t^{0.65}$ [25, 54]. This is due to the connectivity-dominated cage effect as described in Section 2.4.2, where monomers trying to escape are pulled back by the rest of their chain. Below the GT, very little work has been done, but it has been found that diffusive or sub-diffusive behaviour remains possible for *some* particles at temperatures very close to (but below) T_G. There is also evidence for intermittent "hopping" of particles playing an important role in the glassy state [55].

This introduces the notion of heterogeneity. On approaching the GT, certain regions have been found to have much higher mobility than others and the distribution of local displacements is not consistent with a simple Gaussian distribution. One can obtain a picture of this heterogeneity from the self part of the van Hove correlation function [32]

$$G_s(\mathbf{r}, \Delta t) = \frac{1}{N} \left\langle \sum_{i=1}^{N} \delta(\mathbf{r}_i(\Delta t) - \mathbf{r}_i(0) - \mathbf{r}) \right\rangle \tag{2.21}$$

where δ is the Delta-Dirac function. This function essentially represents a probability density of particle displacement over a certain time interval, whose integral over space at any given time is equal to one. In fact, to characterize the distribution of local motion on a given time scale, one can define a non-Gaussian parameter (NGP) in three dimensions as [54, 55, 56]

$$\alpha_2(t) = \frac{3\langle \Delta \mathbf{r}^4(t) \rangle}{5\langle \Delta \mathbf{r}^2(t) \rangle^2} - 1 \tag{2.22}$$

This expression is a good indicator of how heterogeneous the motion is. The

Fourier transform of Eq. (2.21) yields the self part of the scattering function of Eq. (2.19) when generalized for time. The NGP is, in fact, the first correction (of $\mathcal{O}(q^2)$) to the low-q limit of such a function [32]. If all particles are moving in the same manner, then Eq. (2.21) will have a Gaussian distribution and the NGP will be zero. This is true both for diffusive motion (long times) and free particle motion (short times) [32]. A combination of both, however, would yield deviations from a Gaussian distribution. More details as to the utility of such an approach will be discussed in Section 3.3.3.

Furthermore, these fast-moving regions are spatially correlated: they create string-like "cooperative" motion [56]. The fact that mobile regions tend to form near one another is somewhat intuitive, especially when we examine this phenomenon from the free volume perspective. These spatially correlated dynamics have also been studied in the specific case of polymer melts [54, 57]. Briefly, it has been found the chains play an important role in making the motion "string-like," but that there is no evidence for it being along the backbone of the chains themselves. Polymeric glasses behave in a similar way to binary Lennard-Jones glasses (commonly used to simulate fragile glasses), but the distribution of mobile clusters depends on temperature in a different way. Finally, a characteristic length scale of the dynamical heterogeneities has been shown to emerge, thus bringing the GT phenomenon closer to critical phenomena in general, such as gelation. It also has been suggested that the GT is characterized by percolation of "slow" regions [58].

Very little work has been done on the subject of heterogeneity below the GT, however, where we are dealing with non-equilibrium systems. A recent simulation-based study has found that the mobile regions are distributed in a heterogenous way throughout the system (similar to what was seen above T_G) [55]. The clusters of fast particles are more compact below T_G, due to the lack of long-range relaxation. There has also been some experimental work done on the subject, which finds that the fast regions are an integral part of the aging process below T_G [59].

Chapter 3 Model and Calculations

3.1 Statics

We use 3-D Molecular Dynamics (MD) method to simulate a polymer melt at a coarse-grained level. Specifically, we use a bead-spring model to simulate the polymer chains, the neighbouring monomers interacting through a stiff, finitely extensible spring potential

$$\mathrm{U}_{FENE}(r_{ij}) = \frac{1}{2}kR_0^2 \log\left[1 - \left(\frac{r_{ij}}{R_0}\right)^2\right] \tag{3.1}$$

where $R_0 = 1.5$ and $k = 30$ are the maximum spring length and stiffness parameters respectively. These values prevent chains from crossing each other. This type of potential was taken from the work of Kremer and Grest [23], who showed that this potential accurately reproduces static and dynamic properties of polymer systems, as discussed in Section 3.1. More recently, this model has been used extensively by the group of K. Binder *et al.* in order to explore the properties of such systems as the GT is approached from above [25, 26, 37, 38]. In a system similar to theirs, we have assigned 10 beads to each chain and a total of 105 chains (giving $N = 1050$ particles in all). Periodic boundary conditions (PBC) are applied in all directions to reduce finite-size effects. These conditions are applied both during the displacement of particles and during the evaluation of forces.

Polymers can be modelled on various scales, such as that of the individual bonds, the persistence length or the radius of gyration of a chain [29]. Since atomistic resolution is not necessary in order to reproduce large-scale relaxation behaviour, we restrict ourselves to the "mesoscopic" regime [29]. The CPU times required to observe relaxation using atomistic resolution would be astronomical. In the case of polyethylene (PE), for instance, each unit could consist of a CH_2 element. By

coarsening, each unit in our simulations consists of many such segments, since we can approximate such groups as being relatively "rigid" and recover the same large-scale behaviour. Although longer chains would be desirable, it would require that the system size be larger as well, since the chains must be much smaller than the simulation box in order to avoid very large finite-size problems (*i.e.* we do not want a chain to interact with its own image through the PBCs). Furthermore, the relaxation times necessary for a system of long polymers to reach their natural configurations would be very large.

In addition, all particles interact through the truncated and shifted Lennard-Jones (LJ) potential

$$U_{LJ}(r_{ij}) = 4\varepsilon_{LJ}\left[\left(\frac{\sigma}{r_{ij}}\right)^{12} - \left(\frac{\sigma}{r_{ij}}\right)^{6}\right] + C\ , \quad r_{ij} < 2.5\sigma \tag{3.2}$$

where C is chosen such that the potential is zero at the cutoff radius $r_c = 2.5\sigma$. The other relevant units are σ the particle radius and ε_{LJ} the energy scale involved. This type of interaction is crucial for simulating liquids: it contains long-range dipole-dipole induced attractive forces as well as short-range repulsive forces. Furthermore, the combination of both potentials prevent polymers from crossing each other, due to self-avoidance and the proximity of monomers along a chain. At high temperatures, the repulsive part dominates and the attractive "tail" can be ignored. For low-temperature (*e.g.* supercooled) liquids, the same is not true and the attractive part begins to play an important role. Accordingly, we are forced to use a larger cutoff radius $r_c = 2.5\sigma$, which greatly increases computational time. These two potentials provide a competing length scale, which favors the formation of a (fragile) glass, due to geometric frustration. While a pure Lennard-Jones system would tend to form regions corresponding to an fcc structure upon cooling, the optimal chain length is incompatible with any such structure. Fig. 3.1 illustrates this effect by juxtaposing the two potentials. Similar results are found in Ref. [25].

As is generally done in such simulations, the units are non-dimensionalized, defining all quantities in terms of the radius σ, the characteristic LJ energy ε_{LJ} and the mass of a particle m. A recent comparison of experimental PE values with simulation

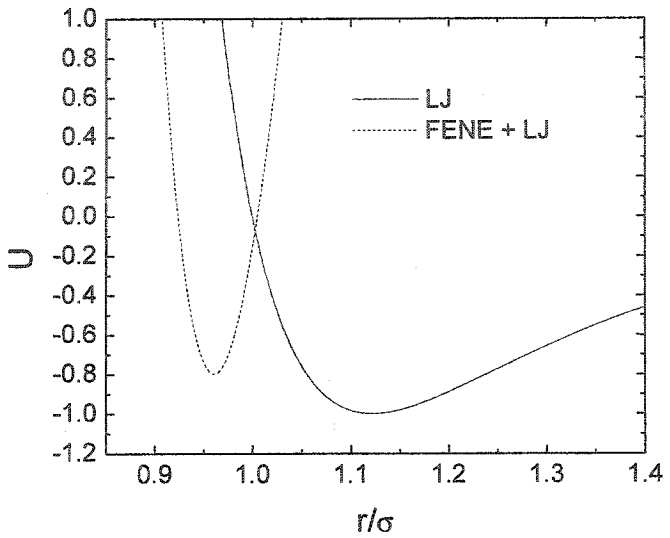

Figure 3.1: The two potentials of Eqs. (3.1) and (3.2) are juxtaposed to indicate the incompatible length scales. The FENE potential has been shifted for clarity.

values using the FENE potential yields the following conversion: $\sigma = 5.3$ Å, $m = 42.3$ g/mol and $\varepsilon = 443 k_B$ K $= 6.11 \cdot 10^{-21}$ J [60]. This yields time unit of $t = 1.8$ ps and a temperature unit of $T = 443$ K. For simplicity, most of the results and methods will be discussed in terms of reduced LJ units.

3.2 Simulating the dynamics

3.2.1 Ensemble choice and isothermal compression

We can approach the problem in a canonical or an isobaric-isothermal ensemble. This does not refer to the actual simulation algorithms, but rather the manner in which we define the thermodynamic state of a system. A purely canonical ensemble, however, resulted in unphysical pressure variations below the GT. Specifically, there was a gradual increase in pressure with decreasing temperature in the glassy phase (see Fig. 3.2), which effectively amounts to

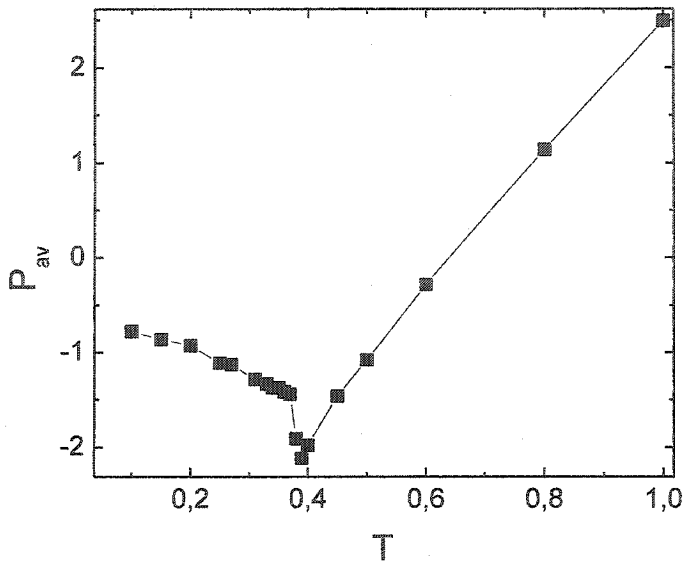

Figure 3.2: Pressure as a function of temperature obtained by keeping volume constant throughout the simulation. Note the sudden rise in pressure as we cool below T_G.

$$\left(\frac{\partial P}{\partial T}\right)_{N,V} = \frac{T}{V}\left(\frac{\partial S}{\partial T}\right)_{N,V} < 0 \tag{3.3}$$

Clearly, this type of entropy variation is forbidden and we must conclude that the system goes through what would have been a two-phase region in the thermodynamic limit (similar results were found in Ref. [38]). For this reason, the results presented henceforth originate exclusively from the isobaric-isothermal (NPT) ensemble. As is discussed in the following paragraphs, the system does not evolve in the NPT ensemble during most of the simulation process. The thermodynamic state used to collect data, however, is defined by an assigned pressure and number of particles at the desired temperature.

One of the main challenges was to generate systems at various temperatures which are in equilibrium or close to equilibrium in the liquid and glassy phase respectively. The most widely-used method is to begin with an equilibrium system at high temperatures and slowly lower the temperature while allowing the system sufficient time

to relax after each decrease [25, 26, 37, 38, 39]. This method has the advantage of allowing data to be collected at different temperatures as the simulation evolves and would likely be the most practical at $T > T_G$. As we approach the glassy phase, the system can no longer re-arrange itself fully. The low temperature does not provide enough activation energy for the system to overcome free energy barriers and "hop" into a new, lower energy basin. This non-equilibrium state is a normal outcome that we wish to investigate. We would, however, like to avoid two related situations: 1) a very high T_G value due to fast cooling rates (as is often the case in computer simulations); 2) systems below T_G, which although non-ergodic, have been unable to explore *any* phase space (*i.e.* have not been allowed to age). For this reason, we propose an isothermal path to enter the glassy phase *via* compression. In this way, the energy landscape is continuously evolving, since we are varying the volume, and the system will eventually find itself in a relatively low basin of the energy landscape. The applicability of this approach is not limited to glassy materials: applying the isothermal compression method to a pure LJ system allowed for faster crystallization than in the case of a simple isochoric path. Although there is a very complete discussion of thermodynamic paths for entering the glassy phase in Ref. [39], it does not specifically discuss an isothermal compression method such as ours.

3.2.2 *Initialization and equilibration*

One of the main challenges in dense polymer melt MD simulations is to have a system that is well-equilibrated. The complexity of polymers compared to, for example, hard spheres or soft spheres, means that the time involved to reach the desired static quantities discussed in Section 3.1 will be much greater. One method would be to generate the system as a series of self-avoiding random walks. This type of method, however, proves to be difficult as the system density increases, and the system would have difficulty reaching equilibrium. Our method, somewhat inspired by the work of Kremer and Grest [23] involves preparing a dilute solution (almost a "gas") of polymers. This was done by separating the system into many small "boxes," each

containing one chain, or occasionally, no chains. The boxes are well-separated, so that each chain essentially evolves alone for some time, reaching its equilibrium R_G and R_{EE}, as defined in Eqs. (2.7) and (2.8) [61]. Furthermore, the initial orientations of the chains are random and periodic boundary conditions (PBC) are applied throughout the simulation.

Once the expanded-volume system is in equilibrium, the system is slowly compressed simply by diminishing the size of the computational box at a rate of at a maximum rate of about $0.015\sqrt{\varepsilon_{LJ}/m}$. We are aiming to create a series of systems at different temperatures but with the same pressure $P = 1.0\varepsilon_{LJ}/\sigma^3$ in order achieve similar results to those of K. Binder's research group [25, 26, 29, 37, 38]. We can therefore estimate at approximately what volume this pressure will be reached. Throughout this process, the system evolves in a canonical (NVT) ensemble. This is realized using the "Langevin MD" method (sometimes referred to as Brownian dynamics), which consists in solving for the following equation of motion:

$$m\frac{d^2x_i}{dt^2} = -\frac{\partial U_i}{\partial x_i} + m\Gamma\frac{dx_i}{dt} - W_i(t) \tag{3.4}$$

This equation contains a Gaussian white-noise source W and a small friction constant Γ which couples the particles to a heat bath. This equation of motion can be effectively used as a thermostat and allows the system to evolve in the NVT ensemble. It has been shown that such an approach is more rigourous than simple velocity-rescaling, for instance [62]. The generalized Fortran implementation was provided by M. Plischke of Simon Fraser University. Briefly, it consists of first generating Gaussian random numbers *via* the Box-Mueller algorithm. Generalized Brownian coefficients can be derived analytically (see Ref. [27] p. 263) and, assuming the algorithm is stable, Eq. (3.4) is integrated by using the coefficients to make an adjustment to the velocity Verlet algorithm discussed in Section 3.2.3. The stability of the algorithm depends on a relatively high value of Γ (we have used $\Gamma = 2$) so that the stochastic term does not dominate.

In order to reach the *exact* volume corresponding to the desired pressure, we employ a damped-force algorithm [27] to realize the NPT ensemble. This method assigns

a desired pressure to the system and, using an external force, expands/compresses the system if the current pressure is too large/too small. The external force is a uniform, 3-D "piston" of mass comparable to that of the system, and under its influence, the system behaves like a damped harmonic oscillator. When the pressure is within the desired tolerance level, the system is given further time to equilibrate before collecting data.

3.2.3 NVE calculations and program structure

In the final part of the simulation, the necessary data is collected in the NVE (micro-canonical) ensemble. When turning off the thermostat, the temperature and pressure were seen to fluctuate around their desired values. The NVE ensemble is the most straightforward when it comes to MD simulations, since no constraints are required; simply solving Newton's equations of motion yields conserved energy. We employ the velocity Verlet algorithm to integrate the equations of motion [27]. Knowing the forces, positions and velocities at the "present" time t, this algorithm involves four main steps. First, we compute the positions at time $t + \delta t$ as

$$\mathbf{r}(t + \delta t) = \mathbf{r} + \delta t \mathbf{v}(t) + \frac{\delta t^2}{2}\mathbf{a}(t) \tag{3.5}$$

where the time step δt is the smallest time unit used to discretize the integration process. Second, we compute the velocities at the *half*-step $t + \frac{1}{2}\delta t$ as

$$\mathbf{v}(t + \frac{1}{2}\delta t) = \mathbf{v}(t) + \frac{1}{2}\delta t \mathbf{a}(t) \tag{3.6}$$

Now we must compute the forces at the step $t + \frac{1}{2}\delta t$ *via* the potentials described in Section 3.1. To evaluate the forces within a chain in Eq. (3.1), each particle has a "tag" indicating which particle(s) are nearest neighbours along a given chain. In this manner, we have only to check the "tag" of each particle and evaluate the forces based on distances to the nearest neighbours. Evaluating the long-range Lennard-Jones forces in Eq. (3.2) which is cutoff at 2.5σ requires some care in order to avoid excessive CPU time caused by checking the distance to all particles. To accelerate

the process, we divide the system into several cubic cells of length $r \gtrsim 2.5\sigma$ and use a neighbour list within each cell [27]. This means that, for a given particle, we need only check its own cell and the neighbouring cells, whose particles can be "scanned" *via* a linked-list implementation connecting one particle to another. The new force values at $t + \delta t$ can be used in the following iteration of Eqs. (3.5), (3.6), but also to finally evaluate the velocities at the next *full* step $t + \delta t$ by a second half-step integration

$$\mathbf{v}(t + \delta t) = \mathbf{v}(t + \frac{1}{2}\delta t) + \frac{1}{2}\delta t \mathbf{a}(t + \delta t) \tag{3.7}$$

where δt has been chosen as $dt = 0.005\sqrt{m\sigma^2/\varepsilon_{LJ}}$. It has been checked that this time step is small enough to ensure system stability. An important effect of the NVE ensemble is that, since the energy is fixed, the system is restricted to only one hypersurface in phase space, meaning that the samples will not age appreciably during the portion of the simulation when data is collected. As well, because we are monitoring very sensitive off-diagonal stress fluctuations, we chose not to use a constant temperature scheme, as the coupling to a uniform heat bath would cause an unphysically fast "decorrelation" to take place.

We assume that our systems are very close to equilibrium. In the liquid phase, this can be checked after having let the system run for a reasonably long time ($\sim 10^7$ iterations). A glass, however, is a system which is *by definition* out of equilibrium. We can say, however, that the glass is not evolving appreciably over the timescales of the simulation, and is therefore close to equilibrium. Given this approximation, we allow the our correlation functions to be evaluated one after the other in time. Typically, we run approximately 400 "correlators" for each sample.

3.3 Collecting the relevant data

3.3.1 Viscosity and time-dependent shear modulus

The stress tensor is computed as [32]

$$\sigma_{\alpha\beta} = \sum_{i=1}^{N} m v_{i\alpha} v_{i\beta} - \sum_{i<j}^{N} \frac{r_{ij\alpha} r_{ij\beta}}{r_{ij}} \frac{\partial U_{ij}}{\partial r_{ij}} \tag{3.8}$$

where the first and second terms represent the kinetic (or ideal gas) and potential parts respectively. The potential part implicitly includes both inter and intra-chain interactions, which combine as U_{ij}. The diagonal elements of $\sigma_{\alpha\beta}$ represent the pressure in the system in its regular sense, while the off-diagonal elements represent the shear stress. Of particular interest is the autocorrelation function of the off-diagonal elements, which gives the time-dependent shear modulus $G(t)$ as defined in Eq. (2.2). We therefore obtain a relatively easy manner in which to calculate $G(t)$ without external deformation [32]:

$$G(t) = \frac{V}{k_B T} \left\langle \sigma_{\alpha\beta}(t_0) \sigma_{\alpha\beta}(t_0 + t) \right\rangle, \quad \alpha \neq \beta \tag{3.9}$$

where t_0 is a given reference time and the average is made over directions, particles (denoted by subscripts i and j) and over time (different reference times). We must recall, however, that the glassy state is non-ergodic: it is restricted to a relatively small area of phase space except, perhaps, on very long timescales. For this reason, the averaging in Eq. (3.9) must not only be done with respect to different starting points t_0, but also with respect to different initial configurations. For this reason, we have used at least 10 completely independent samples for each of these calculations. The same applies to other similar calculations, such as those for diffusion, below T_G.

While Eq. (3.9) appears to be valid in both the liquid and glassy states (it follows from the definition of $G(t)$ itself in Eq. (2.2)), one might wonder whether the same can be said about the viscosity, as computed by the integral of $G(t)$ in Eq. (2.6). The validity of this expression in the liquid state has been rigourously shown, given that the relevant hydrodynamic modes have long wavelengths and low frequencies ω [32]. In this case, hydrodynamic approximations arise from the assumption that the density current (which governs local fluctuations) evolves locally as it would on a slightly larger scale. However, there exists another more simple derivation of Eq. (3.9) which simply considers a small change in the Hamiltonian after a small (shear)

transformation [63]. One can therefore consider the shear stress as a time-dependent response to the perturbation of the Hamiltonian. This approach simply relies on the presence of steady and uniform local shear and does not invoke approximations related to hydrodynamic behaviour. This is important, since at temperatures very close to T_G, the relaxation is dominated by "barrier hopping" or activated processes which are not necessarily compatible with liquid state approximations.

Clearly, the advantage of using Eq. (3.9) over μ obtained from external deformation (see Eqs. 2.1 and 3.13) is that the system remains in its original state. Glasses (as well as many other "soft" or "jammed" materials) are very sensitive to external deformation, which can change the state of the system. Instead, $G(t)$ simply relies on microscopic shear stress fluctuations to obtain the desired information. It also gives us a picture of how stress evolves in time. At $t \to \infty$, $G(t)$ becomes the "equilibrium modulus," G_{eq} and at $t \to 0$, $G(t)$ becomes G_∞, the infinite-frequency modulus [64, 65, 66], as defined in Eq. (2.10).

Eq. (2.6) allows us to obtain the zero-shear viscosity by integrating $G(t)$ to infinity. In the past, viscosity has mostly been calculated in simulation by the imposition of flow and the use of non-equilibrium molecular dynamics (NEMD), in order to avoid the long-time tails of $G(t)$ for viscous fluids (such as supercooled liquids near T_G) [67]. This was resolved by extrapolating $G(t)$ to a KWW or stretched-exponential fit

$$G(t) = G(0) \exp\left[-\left(\frac{t}{t_0}\right)^{\beta}\right] \tag{3.10}$$

where the fitting parameters β and τ can be extracted by rearranging to the linear equation

$$\ln\left[\ln\left(\frac{G(0)}{G(t)}\right)\right] = \beta\left(\ln t - \ln t_0\right) \tag{3.11}$$

and performing a simple least-squares fit, provided the values of $G(t)$ remain above zero. The integral of Eq. (3.10) converges and can be analytically calculated to infinity. This type of fit became less accurate when T becomes extremely close to T_G ($T \sim T_G + 0.02$), since the tails become extremely long, meaning that small errors in the fitting parameters translate into large errors in viscosity. Most importantly,

Eq. (3.10) suggests the presence of dynamical heterogeneity *via* the presence of many different local, exponential relaxation modes which are added together to produce a stretched exponential.

The main problem was being able to distinguish between long tails in $G(t)$ which eventually decay to zero (yielding a finite viscosity) and those which are effectively infinite. Given the short length of our correlators (which was unavoidable due to CPU time restrictions), the long-time behaviour is not necessarily obvious. We have observed that Eq. (3.10) becomes less applicable as we get close to, or below T_G. The slow relaxation of the glass through thermally activated processes is better represented by the power law form, as has been previously observed in gelation phenomena [65, 66]:

$$G(t) = G_{eq} + At^{-s} \tag{3.12}$$

In physical terms, the power law fit uses the distribution of energy barriers explored by the system during the simulation time to predict the long time behavior. This type of fit allows us to extract G_{eq} at very long times, and thus the "true" shear modulus of the system.

3.3.2 Shear modulus from external deformation

We would also like to compute the shear modulus using a direct approach, *i.e.* a response to deformation. The preferred method is to apply a pure shear deformation, which is more rigorous and does not require isotropy or system symmetry to yield accurate results [20]. We start with a cube of side L. For a given strain ϵ_{xy}, an affine shear deformation in the x direction is applied (in a plane with its normal along the y direction). A particle initially in position (x, y, z) is displaced to $(x + \epsilon_{xy}y, y, z)$. The boundaries of the simulation box are also shifted: x_{min} goes from 0 to $\epsilon_{xy}y$ and x_{max} goes from L to $\epsilon_{xy}y + L$. This is applied as a one-time, instantaneous deformation. A schematic representation of the process in shown in Fig. 3.3.

The only difficulty lies in allowing for variable PBCs. For example, given the xy

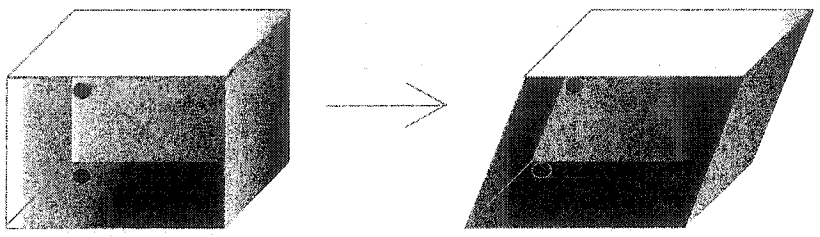

Figure 3.3: Schematic representation of the shear deformation of the simulation box in one direction. The dark circles represent the positions of two particles before and after the system is deformed.

deformation, a particle leaving the top of the simulation box in the y-direction at a x-coordinate x_0 will re-enter the bottom at a position $x_0 - \epsilon y_{max}$. The shear modulus is then calculated with an off-diagonal element of the stress tensor, once the stress has reached a plateau [20]:

$$\mu = \frac{[\sigma_{xy}(\epsilon_{xy}) - \sigma_{xy}(0)]}{\epsilon_{xy}} \tag{3.13}$$

The shearing is applied in the five other directions, substituting xy by yz,$-xy$, etc. Although this part of the simulation was by far the most expensive in computer time, failure to perform this step was seen to result in very poor statistics. Individual samples lack symmetry and therefore the various deformations will not usually give the same stress components. The calculation can also be made without the rightmost term in Eq. (3.13), as per the definition given in Eq. (2.1), but subtracting the "unsheared" off-diagonal stress element at every deformation becomes crucial for statistics. This is simply due to the small stresses present in the glass after the deformation, making $\sigma_{xy}(0)$ non-negligible. Deformations of $\epsilon = 0.01$ to 0.2 were performed, $\epsilon = 0.2$ being close to the maximum allowed instantaneous strain which

does not stretch any bonds past their limit length of $r = 1.5\sigma$ (see Eq. (3.1)).

3.3.3 Measuring movement in the system

We can extract the average diffusion constant D_M of the monomers or D_{CM} of the chain centres of mass through the Einstein relations [27]

$$D_M = \lim_{t\to\infty} \frac{\langle \Delta \mathbf{r}_i^2(t) \rangle}{6t} \tag{3.14}$$

$$D_{CM} = \lim_{t\to\infty} \frac{\langle \Delta \mathbf{r}_j^2(t) \rangle}{6t} \tag{3.15}$$

where we are averaging over the individual monomers i or the centres of mass of the chains j. One can also compute the same quantities by using an equivalent Green-Kubo relation and integrating the velocity autocorrelation function [27]

$$D_M = \frac{1}{3N} \int_0^\infty \left\langle \sum_{j=1}^{N} \mathbf{v}_j(t+t_0) \cdot \mathbf{v}_j(t_0) \right\rangle dt \tag{3.16}$$

where D_M is the average monomer diffusion constant and t_0 represents a given reference time. Note that a similar expression can be made for the centre of mass diffusion D_{CM}. In fact, one can always construct an equivalent Green-Kubo (GK) relation from an Einstein relation and *vice versa*. The advantage of this equation is that, since collisions occur frequently, the velocity autocorrelation function decays quickly to zero and the integral can be reasonably well approximated at short times. We found however, that the statistics associated with the GK form were not very good. Our diffusion measurements are restricted to the forms of Eqs. (3.14) and (3.15). The advantage of the MSD approach to diffusion is that it allows one to observe how far monomers or chains have moved at different times and it can apply to a non-diffusive process, which can be readily observed from the time evolution of the MSD. The presence of non-diffusive processes may be the cause of the poor performance of the GK form. Diffusion measurements were performed in both the NVE and NVT ensembles for all temperatures and the results were identical within error bars, meaning that even in the glassy phase, the system is close to equilibrium.

In order to compute the fraction of mobile particles, we must simply keep track of which particles have moved more than a distance r^*. This can be done using the van Hove correlation function of Eq. (2.21). Assuming isotropy, the function depends only on the scalar displacement r (Eq. (2.21) must be multiplied by a solid angle $4\pi r^2$ to conserve the normalization condition), and can be computed by plotting a histogram of particle displacement. From this, we can extract the fraction of "mobile" particles ϕ as those having moved more than a certain distance r^* in a certain time interval, *i.e.*

$$\phi = \int_{r^*}^{\infty} 4\pi r^2 G_s(r, \Delta t) dr \tag{3.17}$$

Choosing a r^* which is too small would mean including particles which are simply rattling within their cages, while choosing a r^* which is too large would exclude many particles which have successfully escaped from their cages. For this reason, we choose $r^* = 1.0\sigma$, meaning that a particle must cover a distance comparable to its radius, which is similar to an ideal r^* found from a more detailed 2-d simulation [68]. The reader is referred to Appendix A for further details regarding mobile particles. We assume that such a movement is representative of a local relaxation phenomenon.

3.3.4 *Investigating aging phenomena*

If we wish to investigate the aging process in the glass, we cannot restrict ourselves to the NVE ensemble. The "Langevin MD" method used for equilibration in the NVT ensemble does not particularly seem suited to a quenching experiment either. The reason for this is that the stochastic noise term (which essentially simulates the effect of a solvent) allows the system to explore its energy landscape more efficiently. Thus, we are not observing the true relaxation behaviour of the melt. For this reason, we adopt a simple velocity-rescaling method [27]. The equations of motion are integrated in a similar manner as described in Section 3.2.3, but with an additional caveat: after the first half-step velocity calculation, the kinetic energy is computed and the velocities are uniformly rescaled to maintain a constant T. Finally, the second half-

step is evaluated using the rescaled velocities. Recalling that the average kinetic energy per particle, given three degrees of freedom, is $\frac{3}{2}k_BT$, the rescaling factor can be simply computed as $\chi = \left(\frac{T}{\mathcal{T}}\right)^{1/2}$, where T is the desired temperature and $\mathcal{T}$ is the current temperature, as computed *via* the kinetic energy [27]. This constraint is applied approximately every 4 iterations.

If we are looking at a two-time correlation function as in the case of the incoherent scattering function, Eq. (2.20), then we clearly cannot accumulate and average data for this correlation function over many times. It is fortunate that, unlike the stress autocorrelation function, the self part of the incoherent scattering function is relatively noise-free. After an "initial" time $t = 0$ (when a system is quenched, for instance), C_q is evaluated starting from different waiting times t_w. Furthermore, we have implemented an algorithm whereby the "correlators" overlap. In other words, the data collected at one point can correspond to many different waiting times t_w.

To study this decorrelation, we must select a wavevector q close to the main peak of the scattering function $S(q)$, presented in Eq. (2.19). Although any wavevector should show the same type of behaviour [46], the main peak shows a more marked relaxation because it reflects the prominent nearest-neighbour distances. In our case, the only allowed wavevectors have the form

$$\mathbf{q} = \frac{2\pi}{L}(n_x, n_y, n_z) \tag{3.18}$$

where L is size of one side of the simulation box ($\simeq 10\sigma$), and the n are integers. We find the main peak located near $q = \frac{1}{L}\sqrt{51}$ (see Fig. 2.3), meaning that the wavevector can only contain certain integers, such as $\mathbf{q} = (1, 1, 7)$ or $\mathbf{q} = (1, 5, 5)$. We must then average over all the allowed $\mathbf{q}$ values of this form, disregarding the negative values, since we are only retaining the real part of the function (cosine transform).

We also wish to directly study the dynamics of a system which is far from equilibrium. In a similar manner to the generalization of the incoherent scattering function $C_q(t_w, t_w + \tau)$, we propose a two-time MSD to examine the system while it ages. Ordinarily the MSD is defined as $\langle \Delta r^2(t) \rangle$, where $\Delta r(t) = r(t) - r_0$, using only one

reference time for the change in position. This now becomes $\langle \Delta r^2(t_w, t_w + \tau) \rangle$, where $\Delta r(t_w, t_w + \tau) = r(t_w + \tau) - r(t_w)$, which can also be used to compute the two-time NGP $\alpha_2(t_w, t_w + \tau)$ (generalizing the one defined in Section 2.4.4).

Chapter 4 Results: Characterizing the rigidity transition

4.1 Approaching the GT

4.1.1 Characterizing the transition itself

We begin our discussion of results by precisely identifying the GT. Given that the thermodynamic states of our systems are characterized in the NPT ensemble, the most accurate method consists of simply monitoring the volume (or equivalently, the packing fraction) as obtained by the algorithms discussed in Section 3.2.1. This allows us to readily observe a change in expansivity as a signature of the GT, as described in Section 2.3.1. Fig. 4.1 shows how we identify the GT as the intersection of the two slopes corresponding to the liquid and glassy regimes. This very accurate result serves as a benchmark for further analysis of the transition regime. A heat capacity curve, shown in Fig. 4.2 can play a similar role in locating a GT, as discussed in Section 2.3.1. The decrease in C_P upon cooling, however, takes place over a larger temperature interval and it is not clear which part of the decrease should be used to determine T_G, but most seem to place it at the inflection point, somewhere near the middle of the decrease [33]. In this case, the small peak begins at around T=0.55 and the decrease ends around T=0.44. The T_G determined from the expansivity ($T = 0.465$) lies somewhere in the middle of the curve.

It is also worthwhile to briefly re-examine the definition of a GT. As introduced in Section 2.3.1, the viscosity of 10^{12} Pa·s is used experimentally because this implies a relaxation time on the order of 400 s [28]. When we are dealing with simulations, we are working with completely different timescales: the time taken before calculating the volumes of Fig. 4.1 is on the order of $t = 10^5\sqrt{m\sigma^2/\varepsilon_{LJ}}$ or about 10 ns. From

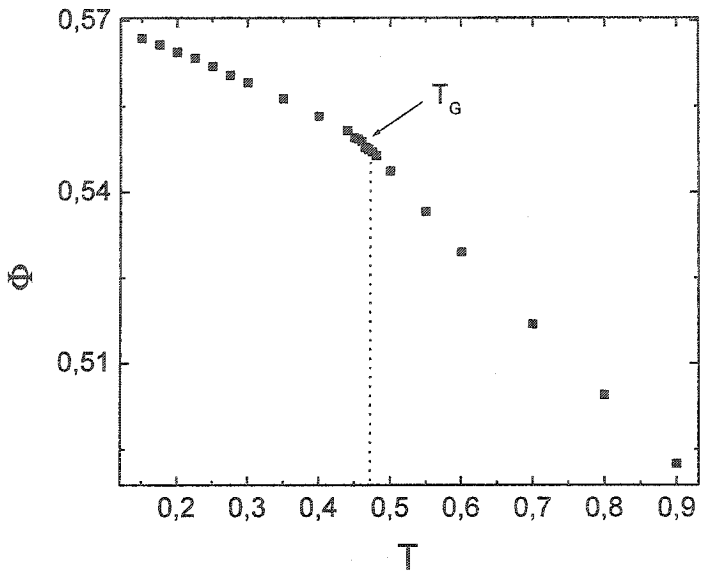

Figure 4.1: Packing fraction Φ as a function of temperature. The intersection of the two slopes in the glassy and liquid regimes accurately determines T_G, shown with the arrow and dotted line.

viscosity measurements (see the following section for details), and using Eq. (2.10), we find that the relaxation time at the GT is of the order of 100 ns, or about one order of magnitude greater than our simulation timescales and 10^9 times smaller than in experiment. Because the GT is a purely timescale-dependent phenomenon and there is no underlying thermodynamic change at T_G, the above timescale is appropriate in our simulation context, and does not change the fundamental physics behind the GT.

4.1.2 *Viscosity*

Having identified the GT, perhaps the most relevant quantity to be measured is the viscosity, which reflects the relaxation possible in the system. We are able to resolve the characteristic increase of viscosity over many orders of magnitude on approaching the GT, along with the theoretical curves of Eqs. (2.14) and (2.17), as shown in Fig. 4.3. The agreement with theoretical predictions seems satisfactory.

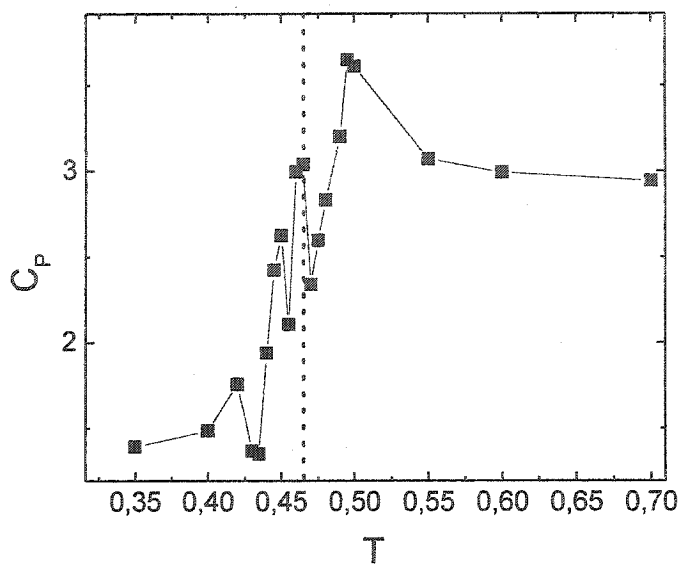

Figure 4.2: Heat capacity C_P found by numerically deriving the enthalpy H with respect to temperature. The dotted line shows the location of T_G as determined from Fig. 4.1. Note that the drop in C_P (as T is lowered) ends around $T = 0.44$, coinciding with the appearance of long-term rigidity.

We also attempted a fit to the MCT approach of Eq. (2.12), which was in fairly good agreement, but not applicable over the same range of temperatures. A summary of these results is shown in Table 4.1.2. The three fitted values (T_C, T_{MC} and T_0) were obtained by adapting and using the nonlinear curve-fitting package of Microcal Origin 6.0©. The results follow the same trends as those of Refs. [29, 38] for a similar system. Our temperatures are only slightly higher, presumably due to the longer range of our attractive LJ potential. Similar viscosity calculations were made during another simulation of this polymer system under flow conditions [67], thus "liquifying" the glass. Not surprisingly, they have found values of T_{MC} and T_0 which were much lower in the case of a driven system.

Table 4.1: The glass transition temperature T_G is presented along with the associated MCT critical temperature T_{MC}, the VFT temperature T_0, and the critical temperature T_C obtained from Eq. (2.17). In addition, we present T_R, corresponding to the onset of true rigidity, found by extrapolation to G_{eq} in Eq. (3.12).

T_G	T_{MC}	T_0	T_C	T_R
0.465 ± 0.005	0.51 ± 0.02	0.41 ± 0.02	0.422 ± 0.006	0.44 ±0.01

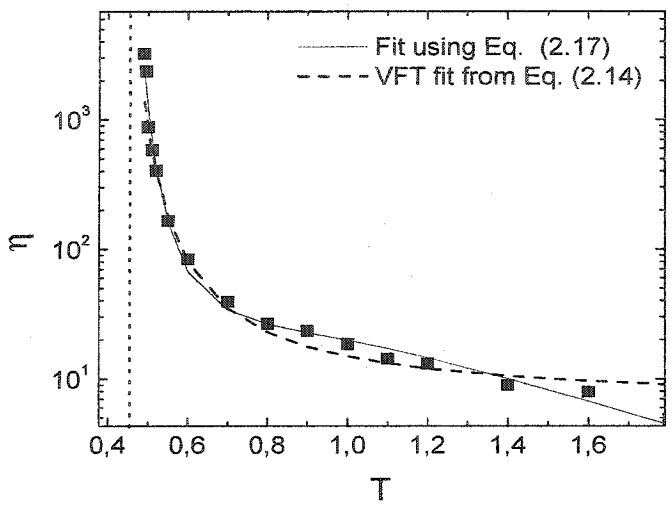

Figure 4.3: Viscosity η above the glass transition, along with the corresponding fits from Eqs. (2.14) and (2.17). The dotted vertical line marks T_G obtained previously.

4.2 The onset of rigidity

4.2.1 *The shear modulus from $G(t)$*

We have also examined $G(t)$, the time-dependent shear modulus, on both sides of the GT. As seen in Fig. 4.4, the main difference between solid and liquid regimes occurs in the long-time tails of $G(t)$. Above the GT, a stretched exponential or Kohlrausch-Williams-Watts (KWW) fit of Eq. (3.10) can be used, while a power law of the form of Eq. (3.12) must be applied for $T < T_G$ [65, 66]. The KWW fit is indicative of a superposition of many different relaxation modes, and possibly some heterogeneity in

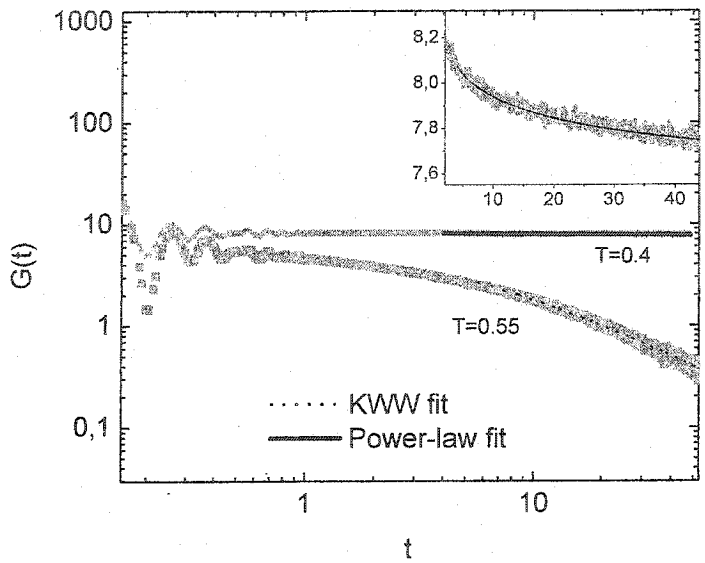

Figure 4.4: Stress autocorrelation function $G(t)$ decay above and below T_G, as calculated from Eq. (3.9). Included are the corresponding KWW and power-law fits from Eqs. (3.10) and (3.12). Note the very slow power-law decay. Inset: Initial decay of the power-law for $T = 0.4$ shown on a linear plot.

the way the shear stress relaxes locally above the GT, which is not surprising, given what is known about the dynamics discussed in Section 2.4.4. The primary goal of computing $G(t)$ however, is to evaluate the shear modulus at long times, *i.e.* the equilibrium shear modulus G_{eq}. We define G'_{eq} as the value of $G(t)$ at the end of our correlation function at a somewhat arbitrary time of $(t = 150\sqrt{m\sigma^2/\varepsilon_{LJ}})$. Although of no special physical importance, the value of G'_{eq} gives some idea of the initial degree of relaxation possible in our system, or the shear modulus at short timescales. However, we would like to examine the "true," long-time relaxation of the glass, which is generally not accessible at simulation timescales. G_{eq} is evaluated at $t \to \infty$ using a non-linear fit to the power-law of Eq. (3.12), giving non-zero values of G_{eq} beginning at $T_R = 0.44 \pm 0.01$, and an approximately linear increase with decreasing temperature, as shown in Fig. 4.5. The decay is generally very slow, meaning that most of the information must be deduced from the initial decay region, as seen in the inset of Fig. 4.4. Similar power-law behavior has been found in colloidal gel

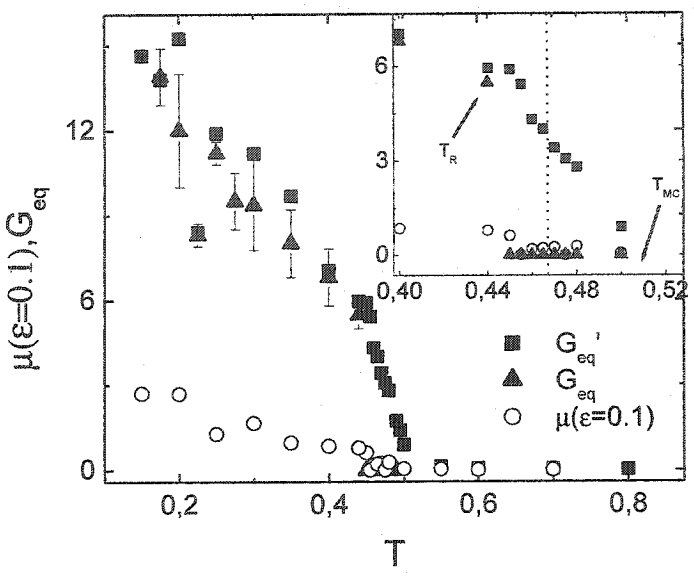

Figure 4.5: Determination of the shear modulus using G'_{eq}, G_{eq} and μ. G'_{eq} is simply the value of $G(t)$ at $t = 150$ time units (the rigidity on very short timescales), while G_{eq} is obtained by fitting the function to Eq. (3.12) at $t \to \infty$. Finally, μ is calculated from Eq. (3.13) *via* a non-negligible deformation of the sample. The inset shows the behavior around the GT (dotted line) with the locations of T_R (the onset of long-term rigidity) and T_{MC} (the MCT temperature) indicated by arrows.

simulations [66]. Although G_{eq} remains an extrapolation based on a relatively small amount of data, we are further convinced of this approach by the apparent change of slope of G'_{eq} at the point where G_{eq} becomes non-zero. G'_{eq} begins acquiring non-zero values at higher T (near T_{MC}=0.51, the idealized MCT temperature). In other words, apparently "solid" glasses can have an almost liquid-like response at longer times, provided the temperature is just above or just below T_G. This is due to the non-ergodicity in the system, which prevents the system from exploring other configurations. Note, however, that the results for G_{eq} cannot put a precise value on the timescale of the long-term rigidity, only that it is much greater than that of the simulation.

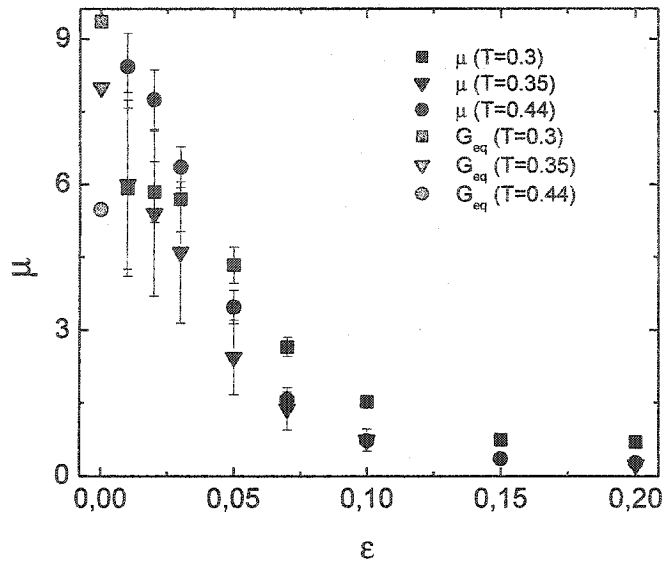

Figure 4.6: Shear modulus μ as a function of shear for three temperatures below the GT. We interpret the G_{eq} as the zero-shear limit to check whether these two methods agree. Note how the statistics get much worse at small ϵ.

4.2.2 *The shear modulus from a finite deformation*

We also compare the G_{eq} results with those directly obtained by shear deformation of the samples (see Eq. (3.13)). The value of G'_{eq} on our short simulation time scales, the value of G_{eq} by fit and the shear modulus from external deformation μ are shown in Fig. 4.5. This preliminary comparison is promising, since both G_{eq} and $\mu(\epsilon{=}0.1)$ begin acquiring non-zero values around the same temperature $T_R = 0.44$. As we would expect, both quantities can determine the onset of rigidity in a system. Clearly $\mu(\epsilon{=}0.1)$ is much smaller than G_{eq}: while G_{eq} calculates the shear modulus *via* the internal fluctuations, μ requires external constraints to be imposed, thus altering the system. We interpret G_{eq} as the shear modulus in the zero-shear limit and therefore, we look for the limit $\mu(\epsilon \to 0)$. Fig. 4.6 shows the function $\mu(\epsilon)$ for a set of samples at three given temperatures. Clearly, this glass displays highly non-linear behavior and we have, as of yet, no *a priori* function with which to fit the points. The limit $\epsilon \to 0$ is computationally prohibitive to reach, since the error

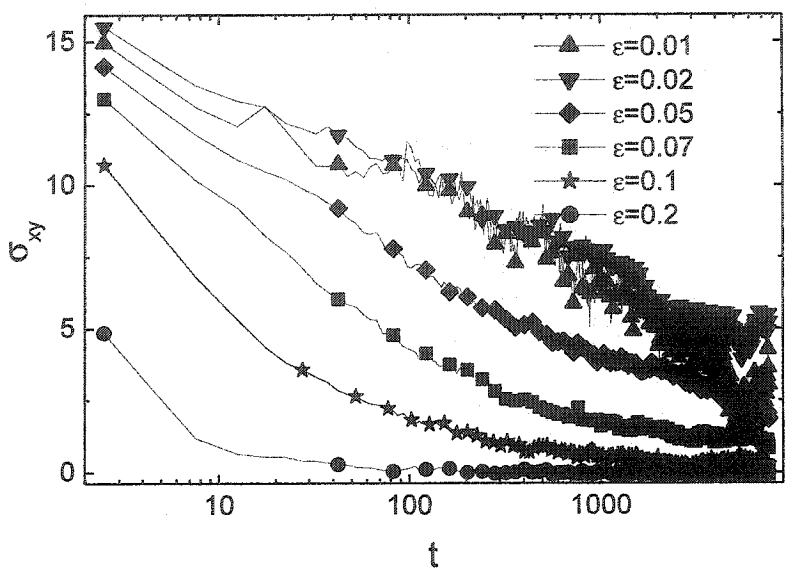

Figure 4.7: Decay of the shear stress σ_{xy} after various initial shear deformations at $T = 0.3$. We can see both the initial stress and the shape of the subsequent decay in the system. Note that for large ϵ there is very little initial stress imparted, followed by a fast decay.

in μ as seen from Eq. (3.13) grows approximately as $1/\epsilon$. Fig. 4.6 does, however, indicate that $\mu(\epsilon \to 0)$ likely tends to G_{eq}. It also suggests that the regime of elastic deformation for these glasses is approximately 2 to 3 %, which is very revealing as to the structure of our fragile polymer glass.

4.2.3 *The effects of deformation on a glassy system*

It is worthwhile to explore the origins of the discrepancy between G_{eq} and μ investigated for a finite shear deformation ϵ. In order to explain the nonlinear behaviour of Fig. 4.6, we examine the appearance and relaxation of the stress imparted on a system subsequent to the deformation, shown in Fig. 4.7. Both the initial stress and the degree of relaxation possible are seen to have significant dependence on ϵ. Applying a large deformation is irreversible, in that the shape of the energy landscape shifts considerably and the system finds itself in a new "well." When a small shear is ap-

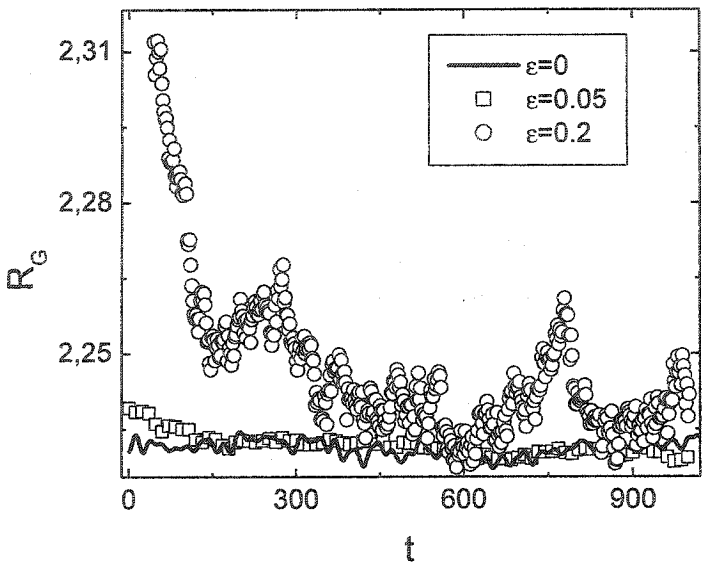

Figure 4.8: Evolution of the average radius of gyration, R_G, of the polymer chains, after a large ($\epsilon = 0.2$) and small ($\epsilon = 0.05$) deformation at $t = 0$ together with the undeformed, "equilibrium" R_G ($\epsilon = 0$).

plied, however, the system remains close to its original configuration. The relatively large residual stress, in this case, is due to ordinary mechanical rigidity (similar to what happens when deforming a crystal, for example). Alternatively, we can analyze what happens on the local level, *i.e.* that of the individual polymer chains in the system. We can view the small/large shear regimes in terms of under/over-extension of the chains. This is seen *via* the evolution of the radius of gyration R_G, as defined in Eq. (2.7), after the application of shear (Fig. 4.8). For small ϵ, the chains are slightly stretched, but are able to recover their equilibrium R_G value quickly. For larger strains, the chains become *over*-extended and do not easily return to their equilibrium value on short timescales.

4.2.4 Shear and aging

In order to investigate the concepts of rejuvenation and overaging we shear the sample and monitor the two-time non-equilibrium function of Eq. (2.20). The tests were

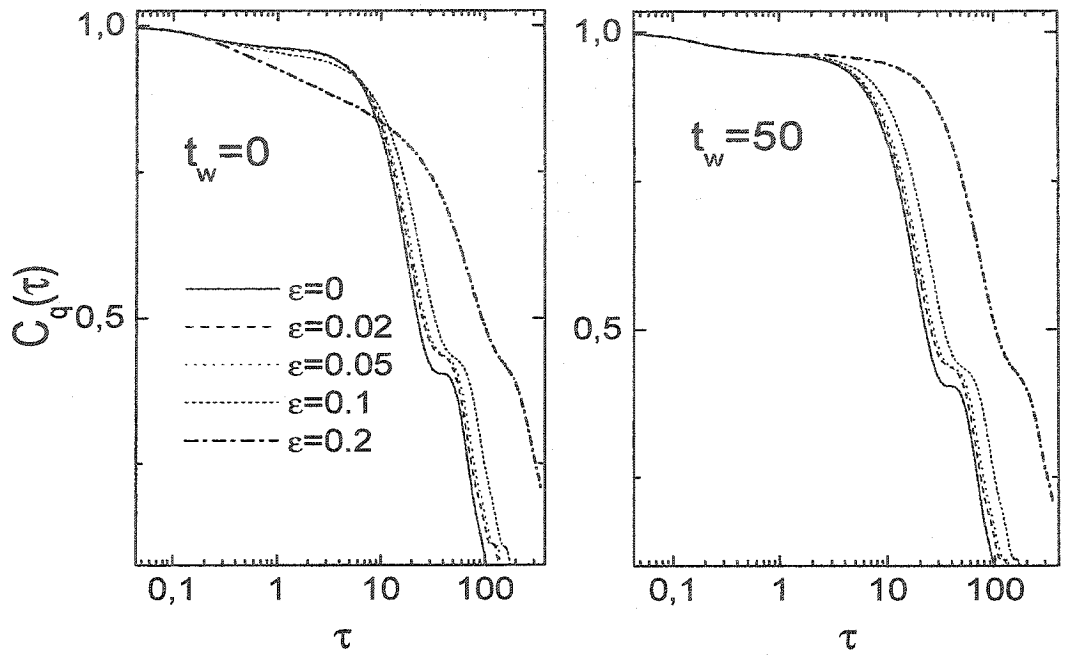

Figure 4.9: Effect of shear on the aging process at T=0.44. Left: The incoherent scattering function $C_q(\tau)$ immediately after the deformation is applied. For large shear ϵ, there is apparent initial rejuvenation, followed by long relaxation times. For small shear there is already a small overaging effect. Right: The same function after a waiting time $t_w = 50$. While there is no change in the behaviour for small shear, the large shear now shows clear overaging. To clarify, at the bottom of each figure and from left to right, the curves go with increasing ϵ (the $\epsilon = 0.02$ and $\epsilon = 0.05$ curves are almost superimposed).

performed for various degrees of shear and for two temperatures: one just below the GT ($T = 0.44$) and a low-temperature glass ($T = 0.275$). Both were found to display identical qualitative behaviour. Recalling that, in this case, the waiting time t_w refers to the time since the instantaneous deformation, the main results are shown in Fig. 4.9. The reference curve represents the no-strain case and shows no evidence of aging for the waiting times studied. Once again, one can separate the "high" from the "low" shear. For a high shear (*e.g.* $\epsilon = 0.2$), we find that immediately after the deformation, the system appears rejuvenated, since the relaxation begins earlier. However, the relaxation is slower. Similar experimental results have been found for

colloidal systems [51] and have been attributed to an initial overpopulation of low-energy states (or relaxation times). We notice however, that after waiting a long time, these states age and we are simply left with an overpopulation of long-relaxation times or unambiguous overaging.

The more surprising results arises from the application of a small or moderate deformation ($\epsilon \lesssim 0.1$). As is seen in Fig. 4.9, the long times appear to be *initially* overpopulated and evolve very little over the course of the simulation. Although the overaging is small for moderate deformations and negligible for very small deformations, such a change in the relaxation of the system is somewhat unexpected.

4.3 Displacement and localization across the GT

4.3.1 *Diffusion on approaching the GT*

Knowing both the displacement of the chains and of the monomers, we can obtain an idea of local motion by comparing the two. We begin by plotting the ratio of the short-time diffusion constants in Fig. 4.10. This is obtained in the method described through Eqs. (3.15) and (3.14), but only retaining the diffusion constant at short times (*i.e.* at $t \sim 150\sqrt{m\sigma^2/\varepsilon_{LJ}}$), which we will call $\mathcal{D}_M$ and $\mathcal{D}_{CM}$. We are therefore not restricted to purely diffusive behaviour, although above T_G the movement *appears* diffusive at short times. This time choice is somewhat arbitrary, but it is important, since it is the same timescale as the $G(t)$ measurements discussed in the previous section. Clearly, we are nowhere near the long-time limit where the "true" diffusion constants D_M and D_{CM} are equal. As we cool towards T_G, the monomer motion becomes increasingly dominant, since the chains become effectively immobile close to T_G. Fig. 4.10 is an illustration of the cage effect: while the motion of chains would require cage-rearrangement, monomers maintain some limited ability to move. This is an important precursor to the system becoming rigid, since the cage effect plays a crucial role in jamming-induced rigidity.

When we look the long-time MSD in the system (Fig. 4.11), so-called sub-diffusive behaviour indicated by the $t^{0.68}$ power-law seems to dominate near the GT (both

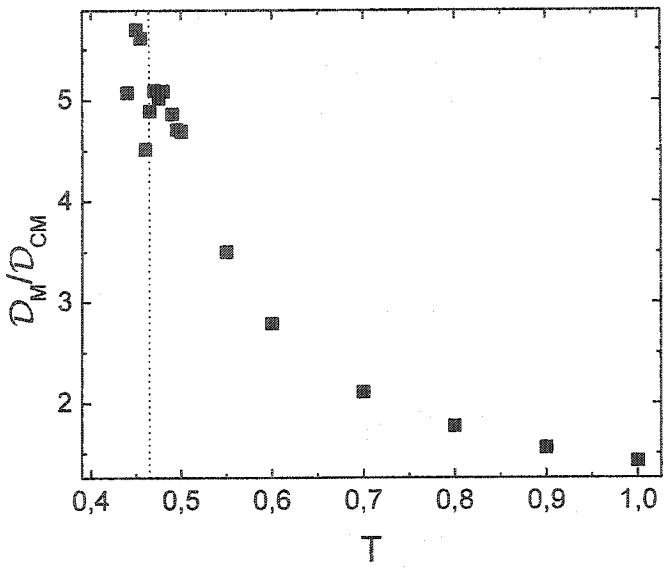

Figure 4.10: Cage effect as seen by dividing the monomer by the chain diffusion constants at short times. The maximum occurs near T_G (dotted line), as the cage progressively "closes in."

above and below it). This is similar to the results found in Ref. [54], and means that cage effect remains dominant for relaxation below T_G. Note that the time scales studied here extend to $t \sim 10^5\sqrt{m\sigma^2/\varepsilon_{LJ}}$, three orders of magnitude larger than the correlation functions discussed in Section 4.2.1. This timescale is close to the limit accessible to simulations. We also plot the long-time displacement of the centres of mass of the chains in Fig. 4.11. As expected, we see no sub-diffusive behaviour in this case, since the cages do not affect the collective motion of the chains. Rather, the chains pass from being approximately static to approximately diffusive with the MSD, scaling as t^1 or $t^{0.9}$.

4.3.2 Movement below the GT

We also examine what type of motion is available to the monomers and chains below the GT. Although very little motion is available to the glass on short times, we can still resolve the short-time diffusion constants $\mathcal{D}_M$ and $\mathcal{D}_{CM}$. Below T_G, these

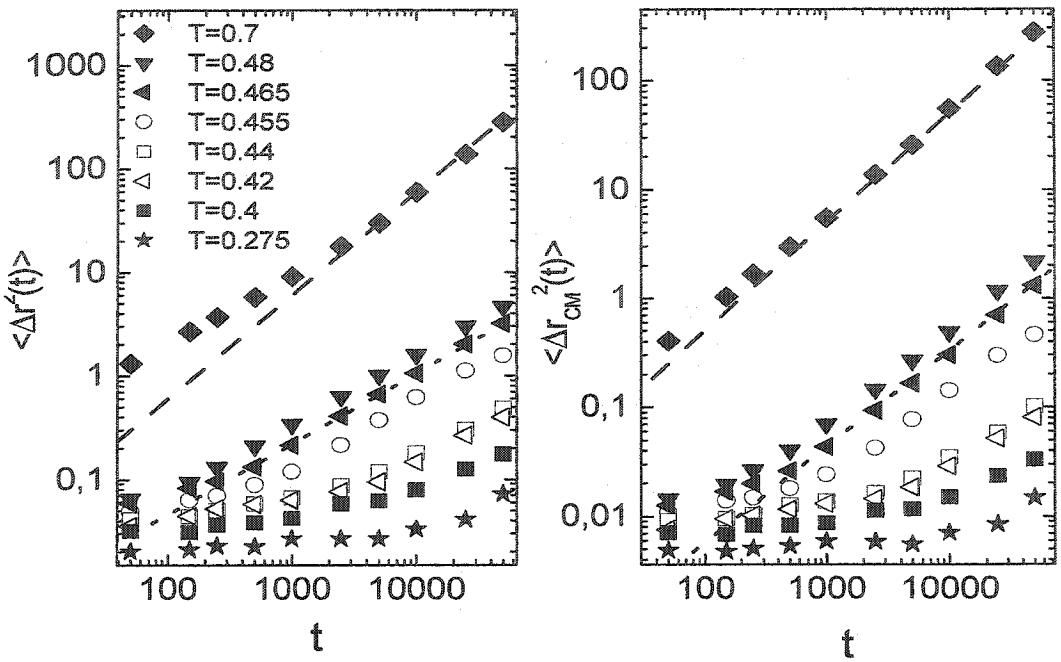

Figure 4.11: Left: The MSD of monomers at long times. The solid and dotted lines are presented as a guide to the eye and are of slope 1 and 0.68, characteristic of diffusive and sub-diffusive behaviour respectively. Note that the onset of sub-diffusive behaviour appears to occur later for $T \leq T_R$.
Right: The MSD of the chain CM at long times (using the same legend). The solid and dotted lines are of slopes 1 and 0.9, showing diffusive or almost diffusive behaviour, as expected, since caging has little or no effect.

concepts seem ill-defined, but remain useful. From Fig. 4.12, we see that virtually no chain motion is possible below the GT, but that the monomers appear to cross-over from being approximately immobile to displaying some motion at around $T = 0.44$ (close or equal to the temperature $T_R = 0.44$ corresponding to the appearance of long-term rigidity). This accounts for the observed stress relaxation in $G(t)$ for $T > 0.44$. However, we would like to investigate the same type of behaviour at long times. Fig. 4.11 seems to indicate that all glassy systems can eventually display some sub-diffusive behaviour, but it appears that the transition to sub-diffusive behaviour occurs at much longer timescales for $T \leq T_R$. We check this by simply monitoring the MSD and the number of mobile particles to see how far the particles have moved over

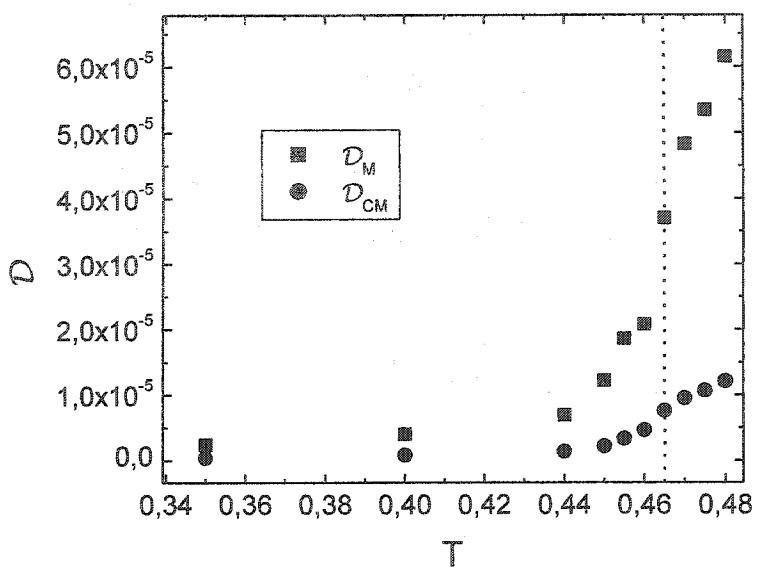

Figure 4.12: Average short-time diffusion of monomers ($\mathcal{D}_M$) and centers of mass of chains ($\mathcal{D}_{CM}$) around T_G. The substantial increase in $\mathcal{D}_M$ begins slightly below T_G (indicated by the dotted line).

different time intervals. The results are shown in Fig. 4.13 and are consistent with the short time results of Fig. 4.12 in that there appears to be a jump in the MSD and in the number of mobile particles (as defined in Section 3.3.3) around $T = 0.44$. This implies that, even in an extremely slow system (below T_G), the MSD (and, in fact, the stress relaxation) is entirely dependent on the movement of a *fraction* of the particles. In addition, this shows that the results pertaining to the rigidity transition are timescale-independent (see Section 5.2.1).

4.3.3 Heterogeneous motion in the system

The non-Gaussian parameter (NGP) $\alpha_2(t)$ (see Section 2.4.4) measures the degree of heterogeneity within the system. It is shown for many temperatures and times in Fig. 4.14. As expected, high-temperature systems have a very low NGP, since the processes are almost purely diffusive after a relatively short time. Around the GT, we see an increase at short times, followed by a decrease. Initially, the motion

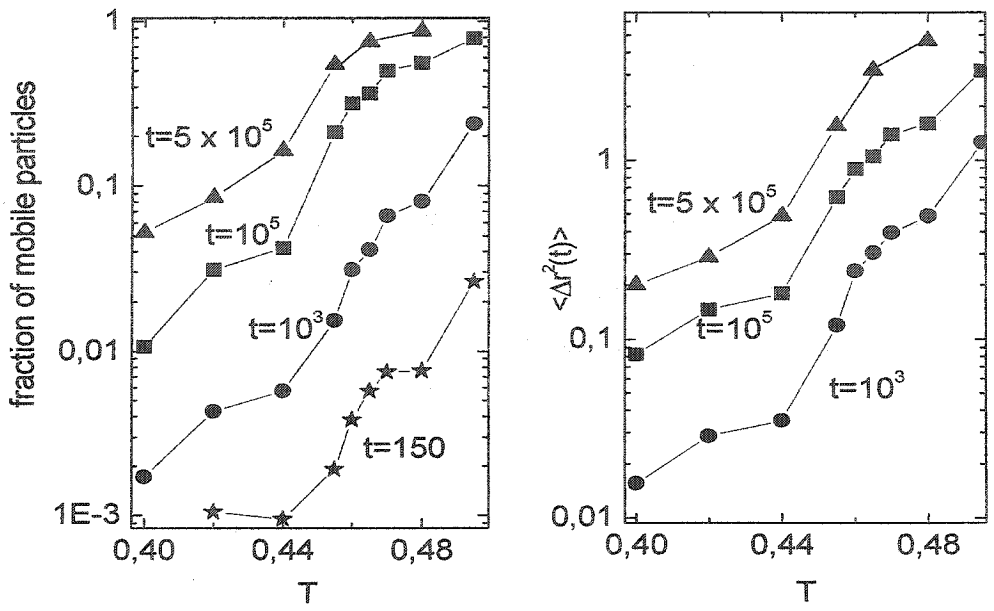

Figure 4.13: The number of mobile particles (left) and the average MSD (right) after different times. Note the apparent "jump" or change in regime around $T = 0.44$ at all times.

is mainly caged and after long times, the motion is primarily sub-diffusive. Similar results have been found for both polymeric and non-polymeric glasses (by simulation and experiment) [54, 55, 69]. In fact, the time when $\alpha_2(t)$ is maximal corresponds approximately to the beginning of the sub-diffusive behaviour of Fig. 4.11 and it has been found that it also corresponds to a maximum in the size of clusters of mobile particles (relative to the particular system) [54]. More importantly, the NGP maxima for $T < T_R$ appear to occur on separate timescales from those at $T > T_R$, indicating that the clusters of mobile particles have much more difficulty developing below T_R. In addition, the final value of $\alpha_2(t)$ (computed at $t = 5 \times 10^5$) is much higher for $T < T_R$, which does not necessarily imply more cooperative movement (see Section 5.2.1). The spatial correlations associated with dynamic heterogeneity are presented in Appendix A. We have seen that the movement in a system near or below T_G is dominated by the movement of particles which escape their cages through collective re-arrangements.

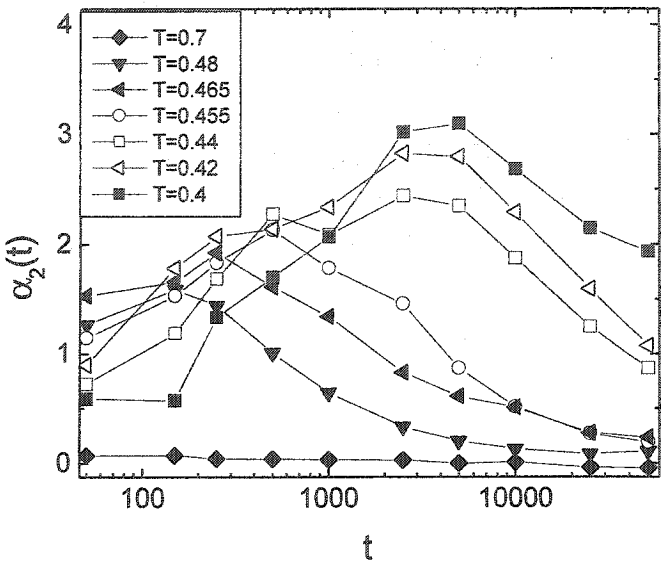

Figure 4.14: Evolution of the NGP $\alpha_2(t)$ for various temperatures. There appears to be a qualitative change in $\alpha_2(t)$ for $T \leq T_R$, as a maximum occurs much later and the final value is much higher.

4.3.4 *Dynamics during aging*

The general slowdown of system dynamics during the aging process is well-documented (see Section 2.4.3). However, we are interested in understanding the local dynamics during the aging process. Fig. 4.15 shows the two-time MSD discussed in Section 3.3.4 after a quench from $T = 1.8$ to $T = 0.275$. As expected, dynamics are seen to slow down as the system ages. For each waiting time t_w, the MSD appears to be constant or very slightly increasing. In order to understand the movement at long times, we perform the same experiment using only one sample and extending τ to much longer times, as shown in the inset of Fig. 4.15. We see that the MSD is punctuated by intermittent "jumps," which dominate the movement during aging. Note that this represents a transient "super-diffusive" process, meaning that the displacements are due to abnormally large movement. The same behaviour can be seen in the number of mobile particles in the system. The degree of heterogeneity given by the NGP $\alpha_2(t_w, t_w + \tau)$ also changes during aging. As expected, the NGP is initially very

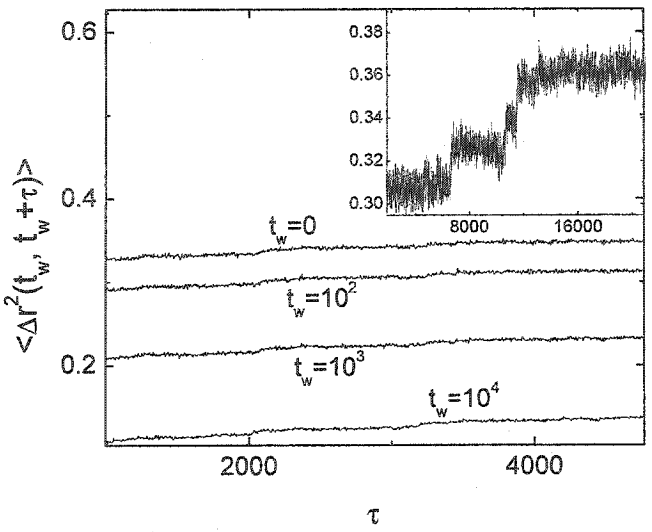

Figure 4.15: Evolution of the MSD for many waiting times following a quench from $T = 1.8$ to $T = 0.275$. As expected, the dynamics slow down during aging. Inset: Example of the MSD for small t_w but longer times τ and using only one sample. Note the sudden increases in the MSD, caused by large, collective rearrangements.

small since the instantaneous quench uniformly slows down the particles which were all previously diffusing (Fig. 4.16). As the system ages, the heterogeneity increases as some particles manage to escape from their cages and clusters of "fast" particles begin to form. Once again, the behaviour of a single sample (see inset) is somewhat more revealing: the NGP displays the same type of jump at short waiting times t_w after the quench. In other words, clusters of mobile particles suddenly appear after a certain time and allow for increased collective movement.

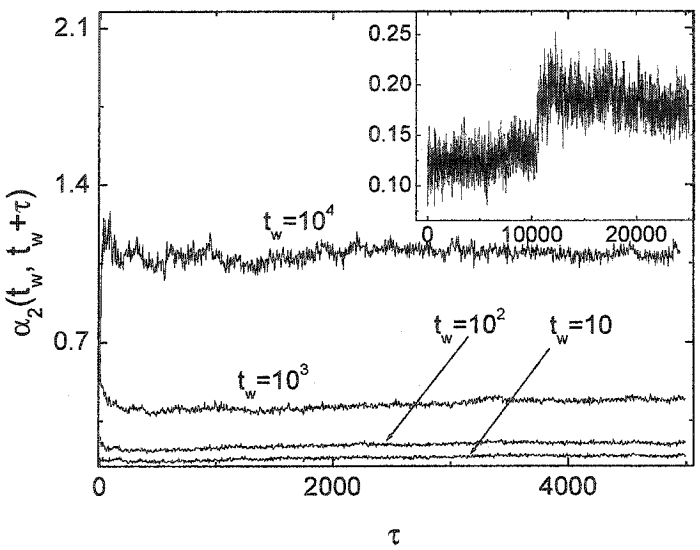

Figure 4.16: Evolution of the NGP $\alpha_2(t_w, t_w + \tau)$ for many waiting times following a quench from $T = 1.8$ to $T = 0.275$. As the system is aging, the dynamics become more heterogeneous. Inset: Example of the NGP for small t_w but longer times τ and using only one sample. Note the sudden increase, whereby the dynamics of the system spontaneously become more heterogeneous and presumably, more spatially correlated.

Chapter 5 Discussion: Rigidity, Dynamics and Aging

In this chapter, we will attempt to give a clear picture of how our system behaves across the GT, based on the results presented and primarily from a rigidity perspective. We will also make a connection with some of the other points discussed, namely dynamic heterogeneity and the issue of overaging / rejuvenation.

5.1 Cooling across T_G

As we decrease the temperature in a supercooled liquid, there are many stages accompanying the process of vitrification and solidification. We first identified the apparent divergence of the "collective" and slow α-relaxation modes at $T_{MC} = 0.51$, following the MCT predictions of a transition to a non-ergodic state. The main consequence of this is not the divergence of viscosity as one would intuitively expect, but rather a change in the way the shear stress decorrelates in the system. The system can no longer easily explore phase space through collective relaxation and must rely primarily on thermally-activated processes to make configurational changes. This theory is consistent with the observed power-law behaviour for $G(t)$ (Fig. 4.4), which does not, however, provide information on the specific dynamics of the system.

Shortly after, we cross the GT at $T_G = 0.465$ and the system falls out of equilibrium. Somewhat surprisingly, we have found that just below the GT, the system is not yet rigid: although the timescale for the relaxation is very large, we can still observe that the time-dependent shear modulus $G(t)$ will eventually go to zero. Therefore, from the rigidity perspective, the GT has no real physical significance. If we take an experimental point of view however, the system may *appear* solid at these temper-

atures. We make the jump from the short MD timescales to the relevant "glassy" timescales of experiment by assuming that the *relative* behaviour is invariant (see Section 4.1.1). So a phenomenon that occurs, say, at 10^{-7}s in our simulations would be occurring on the order of minutes in experiment. The origin of this lack of rigidity lies in the local dynamics. When imposing a very small deformation, the significant amount of local spatially correlated motion is sufficient to let the stress in the *entire* system relax.

The emergence of long-time rigidity occurs at a slightly lower temperature, around $T_R = 0.44$, when the power-law behaviour of $G(t)$ appears to extrapolate to a plateau. However, keeping in mind that the glassy state is out of equilibrium, we cannot state with certainty that the system remains rigid at $t \to \infty$, only that the characteristic timescale of the relaxation becomes *extremely* long. We are further convinced of this result by the change in slope of G'_{eq} (Fig. 4.5), showing that the effects can be seen even after a very short time. Furthermore, the jump in the heat capacity curve of Fig. 4.2 clearly begins before T_G and is, in fact, very close or equal to T_R. This point will be discussed further in Section 5.2.2.

5.2 The origins and nature of rigidity

5.2.1 Rigidity timescales

We have established that there is some type of rigidity transition present at T_R, below the GT. However, we wonder whether this phenomenon is simply a representation of the long "glassy" timescales. In other words, are we simply defining a rigidity transition temperature which depends primarily on the length of the experiment? While CPU time limitations prevent us from computing G_{eq} at much longer times, the mean-square displacement curves are also a good indicator of a rigid system. The results presented in Section 4.3.2 show that, as we increase the length of the simulation by many orders of magnitude, the same change occurs at T_R: particles pass from being almost entirely localized to semi-mobile, as shown in Fig. 4.13. Similar jumps or shifts in behaviour have been observed in glassy systems, but none

of these have been able to relate such a phenomenon to rigidity [70, 71]. While Angell [70] describes such a shift as a "trigger" to a GT, Luo [71] attributes slower diffusion to the dominance of local "hopping." A related time-dependent phenomenon introduced in Section 4.3.3 occurs when mobile clusters are largest and $\alpha_2(t)$ reaches a maximum. This correlated, heterogeneous movement (see Appendix A) can allow the stress to be eliminated in a system. In other words, the cages must be re-arranged: motion within the cages is not sufficient for total relaxation. We have noticed that within the temperature range $T_{MC} > T > T_R$, the peak in $\alpha_2(t)$ (Fig. 4.14) and the onset of sub-diffusive behaviour are slightly delayed as the temperature is lowered. When the temperature passes below T_R, however, this characteristic time increases considerably, as shown in Fig. 4.11. One might infer that the very high peaks in the NGP (after long times) below T_R imply the formation of very large mobile clusters. Recent simulations have shown, however, that in the glassy phase, there are more clusters (hence the high NGP values and the large peak in Fig. A.3), but that the clusters are much smaller [55, 72]. We believe this to be especially important for $T < T_R$, and the "compactness" of the clusters means that there can be no *large-scale* relaxation. Based on the long-time behaviour of the MSD, NGP and fraction of mobile particles, we can safely conclude that our establishment of a rigidity transition at $T_R = 0.44$ is not purely timescale-dependent.

5.2.2 Constraints, self-organization and floppy modes

The rigidity investigated is better described by the presence of cages than by the presence of bonds. The chemical bonds within chains clearly have the effect of "solidifying" the cages, by preventing single-particle escape. The van der Waals bonds, however, are too weak to be considered explicitly as constraints. The induced dipole-dipole moments represented by the attractive part of the LJ potential in Eq. (3.2) are dominant only for unconnected particles, and only at a distance close to $2^{1/6}\sigma$. Nevertheless, the attractive potential plays an important role in *keeping* the cages together for a longer time.

This being said, the lack of chemical bonds does not prevent us from using some of the concepts described in Section 2.1, which are generally only applied when explicit constraints are present. It is therefore useful to consider that they are *implicity* present in our system. Finding a satisfactory method to unambiguously count constraints (in a similar manner as is done in network glasses [3, 4, 14, 15, 16]) has proven difficult. First, one must define a radius which clearly characterizes a bond. Second, one must consider a minimal characteristic "bonding time" before particles can be considered bonded.

From the perspective of constraints, the most important characteristic of the glassy state is the manner in which the rigidity develops in the system [3, 4]. If we rely on results pertaining to simulations of both purely repulsive and "sticky" hard sphere fluids [4], then rigidity is not allowed to spread in glasses by avoiding the formation of over-constrained regions. We believe that this can be applied to glasses formed by jamming in a general manner, meaning that the average number of *implicit* constraints cannot be higher than 2.4, which is the value favouring glass formation [73]. This is due to our competing length scales, which cause the required number of particles to form a given cage, even at very low temperatures. This is a seemingly paradoxical effect since, as we lower the temperature below T_G in our NPT ensemble, the volume decreases as well and one would expect that the number of constraints would greatly increase. This cannot be the case, however, since over-constraining would lead to rigidity nucleation. Therefore, the particles are further "jammed" while minimizing the number constraints, although obvious structural changes do not appear in the radial distribution function. It would be interesting to investigate the details and the mechanism behind this phenomenon.

We can also use the notion of free volume in an analogous manner as the constraints. We postulate that the RT occurs when the local free volume is lower than a critical value v^* in our glassy system. Such an approach to characterize the GT has been proposed by Colby [30] (briefly explained in Section 2.3.5), and we believe that it extends to the RT as well. This type of approach seems attractive for two reasons. First, it takes into account the presence of heterogeneous dynamics in the

form of "cooperatively rearranging regions." Second, it provides a framework which is very similar to the percolation-based explanations of the RT in gels [12, 19]. Many similarities between glasses and gels have recently emerged and it seems natural to assume that they obey similar types of scaling laws as they become rigid.

The rigidity transition at T_R can also be interpreted from a thermodynamic perspective. The end of the decrease in C_P (Fig. 4.2) suggests the establishment of a state with different (configurational) entropy, *i.e.* with many less modes accessible to the system. As a guide, we can relate the entropy to the heat capacity *via* [7]

$$\left(\frac{\partial S}{\partial T}\right)_P = \frac{C_P}{T} \tag{5.1}$$

Therefore, a change (with increasing temperature) from a small to large slope around $T_R = 0.44$ means that a small temperature change can allow for many more available configurational states. This does not imply a true phase transition at T_R any more than at T_G, but from a rigidity perspective, the sudden rise of C_P has great importance. It is worthwhile to mention the connection between floppy modes and the energy landscape. We can also associate the number of floppy modes with the number different configurations available to the system at a given T or, in other words, the number of similar energy basins in the landscape [74, 75]. This seems intuitively correct: a liquid, for instance, would have $f \gg 1$ corresponding to a huge quantity of equivalent energy configurations. In the opposite case, a true crystal which is over-constrained (*i.e.* $f < 0$) has no other similar configurations, since it constitutes a unique state. The rise at T_R is, in fact, due to the contribution of floppy modes, which allow the system to deform without energy cost. The relationship between C_P and floppy modes has been studied in the case of network glasses: the jump in C_P coincides with the well-known coordination number of 2.4, the point where there are very few floppy modes present [74]. While the shape of C_P is familiar to those studying the glass transition, an interpretation based on floppy modes has, to our knowledge, never been used without explicit constraint counting.

5.3 The jamming phenomenon

It is clear that the RT can be described as a "jamming transition" in the case of a glass dominated by repulsive effects. The cage effect plays a dominant role (replacing chemical bonds, for instance) in inducing rigidity. Although the large error bars prevent an accurate fit, the system's rigidity appears to increase with decreasing temperature below T_R, as seen in Fig. 4.5. This is also due to the presence of cages: increased temperature in the NPT ensemble causes them to increase in size and decrease in stability. Generally, glasses will be more rigid (less "soft") than gels, because the shear modulus should have an inverse dependence on the length of the "elementary mechanical unit" [43]. While this unit is simply a particle in glasses, it would represent some type of cluster in most gels. Another unique property of glasses is the aging phenomenon, which is not seen in gels. However, as we have stressed throughout this thesis, the ability of the jammed state to unify glasses and gels is much more striking [18]. Given identical systems (with some attractive interaction potential), gels have been seen to form primarily at low densities, while glasses tend to form at high densities, with both displaying similar relaxation behaviour [76].

Applying a deformation gives further insight into the jammed system's rigidity. From Fig. 4.6, we have shown that $\mu(\epsilon)$ likely tends to G_{eq} in the limit $\epsilon \rightarrow 0$, but that G_{eq} is also much more accurate, given the large error bars associated with μ at small ϵ. When we compute the $G(t)$ from local stresses or when applying a very small deformation, there is no substantial change in the system: the large residual stress arises from the system attempting to return to its original configuration. We can infer that this is primarily a mechanical rigidity phenomenon, as in the case of a crystal. In contrast, applying a large deformation over-stretches the chains and the system moves to a different potential energy well. The smaller restoring stress is due to the fact that, on average, the *undeformed* system is in a relatively deep well and after deformation, the new well will generally not be as deep. The presence of chains in the system also allows for some non-negligible entropic rigidity contribution when applying a large deformation. As Fig. 4.8 has shown, there is a clear initial extension

of the chains. This is followed by a partial relaxation towards their equilibrium length because the lack of permanent bonds between chains allows them to "slip" as the cages rearrange. For this reason, the entropic contribution is not as dominant as in the case of vulcanized rubber, for instance [11]. In the context of the "soft glassy rheology" model (Section 2.4.3), the behaviour depends on how the local minima are distributed across the energy landscape in terms of their depth. This will essentially determine how much local strain is required to shift the system into a new minimum and rearrange the particles accordingly. We propose that instantaneous shear deformations could eventually be used to determine the fragility of the glass in a quantitative manner by revealing the shape of the energy landscape.

5.4 Comparison with GT theories

In Section 2.3, we introduced various competing theories which attempt to explain the phenomena associated with the GT. There has been much controversy over the validity of these competing theories [6, 29]. We have focused on the divergence of the viscosity η (or relaxation times τ), since this should be equivalent to a true RT. In Section 5.2.2, we commented on the apparent advantages of Colby's dynamic scaling approach. We should also discuss the relevance of the fits performed to Eqs. (2.14), (2.12) and (2.17), which predict viscosity divergences at temperatures T_0, T_{MC} and T_C respectively and are presented in Table 4.1. Below T_G, it becomes difficult to access the "true" equilibrium state of a system due to the slow dynamics. In addition, we cannot accurately measure the viscosity of the unperturbed system much below T_{MC}, due to the tails of $G(t)$ becoming excessively long. Therefore, the predicted viscosity divergences at T_0 and T_C remain extrapolations and their physical relevance is questionable. It has been found, however, that the proximity of T_0 to T_G is very useful to characterize the fragility of the glass [6, 40]. It should be noted that while the values of T_0 and T_C are slightly smaller than T_R, they are not inconsistent with it, given the error bars. Therefore, a connection could exist between the extrapolated divergences (at a hypothetical equilibrium state) and the measured onset of rigidity

in a non-equilibrium state. More work is required to understand the relationship between the equilibrium extrapolations and the non-equilibrium measurements.

The idealized MCT temperature is simply a precursor to the GT, in that it only deals with the slow α-relaxations. Their divergence marks the very important ergodicity-breaking (which we have observed) and the appearance of short-time rigidity, as well as being the main contribution to the loss of equilibrium at T_G.

5.5 Glassy dynamics and stress relaxation

As expected, the dynamics of the system are closely related to its ability to alter local stress. A sudden decrease in the MSD with decreasing temperature is an equally good indicator of a RT, since any substantial translation of a particle (beyond its cage limits) will effectively allow for stress relaxation. The interest here is in how the dynamics allow a system to remain *non*-rigid above, but close to, T_R. Collective, correlated motion is the only way for a large-scale re-arrangement of the cages to take place and move the system into a lower energy configuration. The power-law decay observed for $G(t)$ (Fig. 4.4) essentially "samples" the distribution (over a relatively short time) of the potential energy barriers, which are assumed to be more or less constant, and we then use this information to extrapolate to G_{eq}. The power-law relaxation towards zero at $T_G > T > T_R$ likely reflects the large-scale collective rearrangements which allow the system to "hop" over free energy barriers, and are possible due to the presence of excess free volume. The *explicit* relationship between general activated processes and collective motion, however, remains unclear.

The "jumps" observed in the MSD after a quench show the existence of intermittent events, similar to those previously observed in the relaxation *via* the incoherent scattering function [46]. Each "jump" allows the system to move into configurations which correspond to the *equilibrium* configurations of progressively lower temperatures. While the collective rearrangements imply a sudden increase in movement, they ultimately allow the system to achieve slower dynamics by moving the system into a lower potential energy well. In this sense, such observations have important im-

plications for the rigidity of the system. When the system undergoes a large quench, the catastrophic events and their effects are easily measured. Most of our experiments below the GT were performed on systems which are out of equilibrium, but which have already been allowed to age considerably, thus bringing them closer to an equilibrium state. The non-zero rigidity moduli observed for $T \leq T_R$ imply that the system does not undergo any "catastrophic" events to "decorrelate" the local stresses. However, it is likely that such events *can* still occur, but are very rare. Once again, this brings us back to the notion of large timescales when dealing with the rigidity of glasses. Our results also confirm recent experimental evidence that the aging process is dominated by heterogeneous dynamics [59].

5.6 Shearing and the aging process

As we have previously discussed, a system far from equilibrium is able to get rid of excess entropy through the aging phenomenon. Naturally, the progressive slowdown of dynamics implies that the system will become more solid with time. When a system has aged considerably, it becomes difficult to observe this slowdown on "reasonable" timescales and the system appears to have a constant shear modulus over very long times.

From a practical standpoint, it is interesting to investigate whether one can alter the dynamics of a system simply by deforming it. While applying a constant shear flow will clearly "liquify" the system and wipe out its "memory" as glass, we have seen very different effects after a one-time deformation. We have reproduced the experimental results (for a very different type of glass) of Ref. [51], finding that a one-time large deformation causes a partial rejuvenation, followed by overaging, as the system finds its new metastable state. Any small or moderate deformations ($\epsilon \leq 0.1$), however, have a different effect: they cause a small instantaneous overaging, which persists a long time after the deformation. In other words, it is possible to slow down the dynamics very quickly by applying a sequence of one or more deformations. We believe that such a process can, up to a point, "jam" the glass even

further and allow its structure to become more rigid. Furthermore, it is clear that overaging can be useful if one wished to prepare a glassy sample, experimentally or by simulation, whose characteristic relaxation time is much closer to its projected equilibrium relaxation time.

Chapter 6 Conclusion

In this thesis, we have examined the rigidity of a fragile glass former, modelled by a molecular dynamics simulation of a polymer melt with van der Waals interactions. We have established the presence of an apparently timescale-independent rigidity transition (RT) at $T_R = 0.44 \pm 0.01$ below the glass transition (GT), which occurs at $T_G = 0.465 \pm 0.005$. This rigidity transition is characterized by the appearance of a non-zero equilibrium shear modulus G_{eq}, computed by extrapolating the time-dependent shear modulus $G(t)$ to $t \to \infty$. This calculation, performed near equilibrium, is compared to the shear modulus μ, as obtained following a one-time shear deformation. Both methods appear to be in agreement, although it is found that computing μ is less practical and that large deformations have a non-negligible effect on the system structure and dynamics.

We have incorporated a variety of numerical techniques in order to simulate the system in many thermodynamic ensembles and minimize the required computational time. We have used a model that has been shown to accurately reproduce many important properties of polyethylene [60] and, most importantly, is able to model a fragile glass-former using competing length scales. The calculations performed at $T < T_G$ constitute the main novelty of this work. We have found that satisfactory computations of $G(t)$ as a Green-Kubo formula can be applied, provided correct averaging is used in a non-ergodic system. Although not in equilibrium, care has been taken to ensure that the glassy states are *stationary* over the relevant timescales. When necessary (*i.e.* when far from equilibrium), we have generalized quantities such as the incoherent scattering function, the mean-square displacement and the non-Gaussian parameter to "two-time" functions.

Generally, the GT is interpreted as a dramatic slowdown of the dynamics and

transition to a non-equilibrium state, in addition to which we resolve an important dynamical transition at the RT. Specifically, the lack of free volume dramatically reduces the ability of the particles to move large distances, thus preventing stress relaxation. Furthermore, we have established a qualitative change in the heterogeneous and spatially correlated dynamics at the RT, indicating that cooperative rearrangements are responsible for the slow relaxations in the glassy state above T_R. Such collective motion has also been seen to be the driving force in the aging process, as the system slowly "discards" its excess free energy in a series of "catastrophic" events. In addition, we have resolved two distinct effects of a one-time shear on the system's age: a large shear results in a transient combination of rejuvenation and overaging, which has been previously observed [51], while a small shear results in a small and instantaneous but seemingly permanent overaging effect.

While the rigidity of a glass presents clear differences from that of a crystal (*e.g.* in the way the rigidity organizes within the system), we chose to assume implicit constraints due to the caging or "jamming" of the particles. We therefore make use of concepts commonly associated with mechanically-constrained systems, such as that of "floppy modes" to explain an increase in the heat capacity C_P which begins at the RT. We have also compared the observed RT to various theories predicting viscosity divergence below the GT. Some interesting similarities have been established, especially with a recent dynamical scaling approach [30], but we cannot comment with certainty on the accuracy of such theories, due to the non-equilibrium nature of the system below T_G. It does seem clear, however, that the plethora of apparently valid theories explaining the GT reflects the lack of a complete, all-encompassing understanding of general GT phenomena [5, 6, 29]. We suspect that the GT or RT is characterized by a percolation of relatively "slow" or "fast" regions, as was recently observed for very specific systems [58], but a more rigorous examination of heterogeneous dynamics than that of the present thesis would be required. Alternatively, one could examine the system in terms of localization lengths [77] as an order parameter to determine the presence of critical phenomena around these transitions

Currently, there is a large effort underway to group the fluid-solid transition in

materials such as glasses and gels as general "jamming" transitions [18, 41, 42, 43, 72, 76]. This avenue of research seems promising, since many similarities between different jammed states have become apparent. As we have pointed out, however, there are many properties related to rigidity which, so far, appear to be unique to the glassy state. Further research into fragile glasses (generally containing few or no bonds) should develop a coherent method to define the constraints caused by caging, thus allowing for an unambiguous comparison between network and polymeric glasses, for instance. More generally, a rigorous, quantitative definition is required to identify the jammed state, since current arguments (except for recent applications of MCT to colloidal gels [76]) are generally qualitative in nature [18].

Appendix A Spatially correlated dynamics

Knowing that both diffusive and caged motion can coexist in the same system, we investigate how this type of motion is distributed in the system. One can obtain a simple picture of how the "mobile" particles (as defined in Section 3.3.3) are spatially correlated. Fig. A.1 shows a typical distribution of displacements for a system at $T = 0.465$ at two different times, computed using the van Hove correlation function of Eq. (2.21). Notice that at short times, there are hardly any mobile particles and the distribution is Gaussian. At later times, the Gaussian becomes skewed, due to particles escaping their cages.

We also notice that the mobile particles are not distributed randomly in the system, as is shown in Fig. A.2. This figure presents snapshots of the mobile particles in the system corresponding to different values of the NGP α_2. We have used two different temperatures ($T = 0.44$ and $T = 0.7$) and, for clarity, we have chosen different times to have approximately the same number of mobile particles in each system. Although both systems seem to show some "clustering," one can see that the increased heterogeneous behaviour also implies increased spatial correlation, but non necessarily increased *size* of clusters. This has been found in many different glass-forming systems [52, 55, 56], but the effect is amplified by the extra connectivity in a polymer system [54].

To quantify these correlations, we can compute the RDF of mobile particles, applying Eq. (2.9) to only the mobile particles around the first peaks only. This is done at three different temperatures, but using the same elapsed times to locate the mobile particles. We notice that for a high NGP, the nearest neighbours of a mobile particle also tend to be mobile. This seems intuitive for the nearest neighbours along a chain (peak), since a particle cannot move without "dragging" its neighbour.

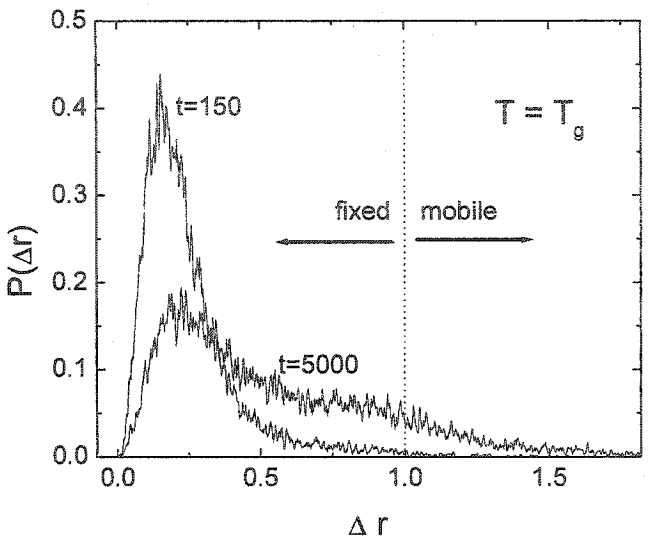

Figure A.1: Typical displacement probability densities at short and long times averaged over 10 samples at T=0.465. The dotted line indicates the distinction between mobile and immobile particles as a displacement greater than 1.

We also see similar, but less marked, behaviour for the second peak corresponding the LJ length scale. The polymeric nature clearly has an important effect on the heterogeneous dynamics, but the same type behaviour would persist without the chain connectivity, as has been found in other systems [52, 56].

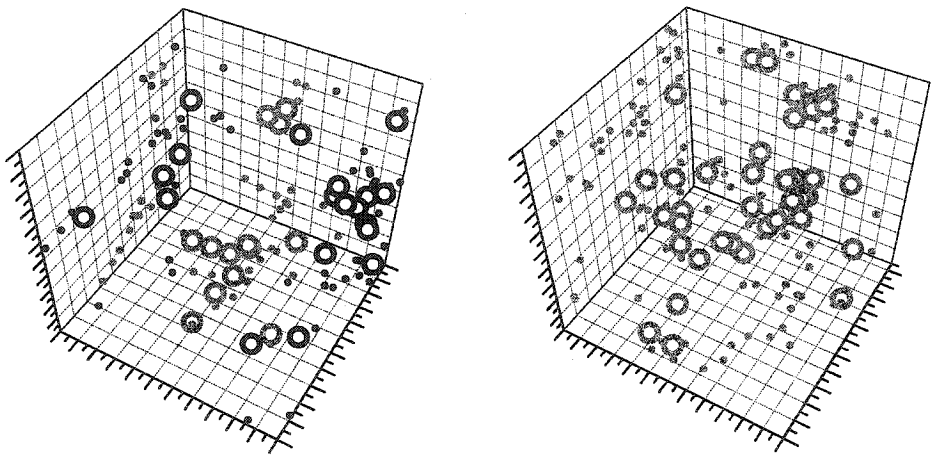

Figure A.2: Snapshots of mobile particles within a cubic system. Left: Two different samples (grey and black circles) at $T = 0.44$, $t = 5000$. Right: Mobile particles at $T = 0.495$, $t = 150$. The NGPs ($\alpha_2(t)$) for the left and right systems are 2.5 and 0.85 respectively. The small circles are projections in each plane (as a guide to the eye). Note the increased spatial correlation for the system with higher NGP.

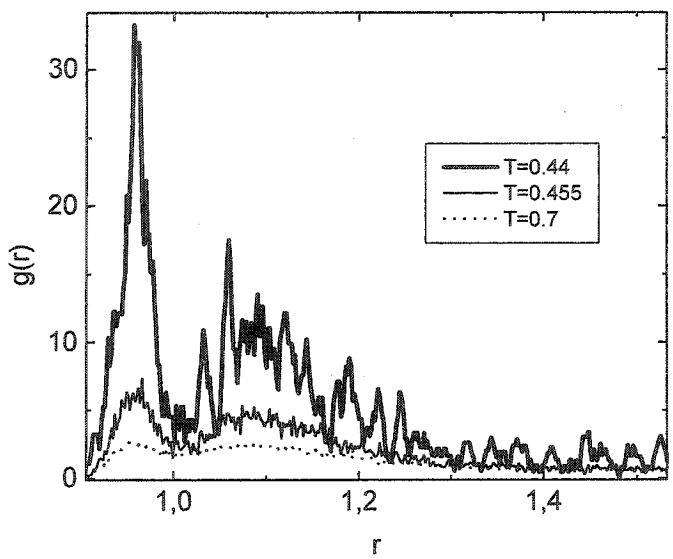

Figure A.3: The RDF of the mobile particles at three different temperature after $t = 10^5$ time units. The curve of $T = 0.7$ corresponds is very similar to an RDF which considers *all* particles, due to the lack of spatial correlation.

Appendix B Glossary of Symbols and Acronyms

B.1 List of Roman letter symbols

$\mathbf{a}$	Acceleration
$C_\mathbf{q}$	"Self" part of the incoherent scattering function
C_P	Heat capacity at constant pressure
C_V	Heat capacity at constant volume
f	Fraction of floppy modes in the system
D	Diffusion constant
$\mathcal{D}_M$	"Short-time" diffusion constant of the monomers
$\mathcal{D}_{CM}$	"Short-time" diffusion constant of the chains' centres of mass
E	Energy
E_{act}	Activation Energy
$g(r)$	Radial distribution function
$G_s(\mathbf{r}, \Delta t)$	van Hove correlation function
$G(t)$	Time-dependent shear modulus
G_{eq}	Equilibrium shear modulus
G'_{eq}	Short-time equilibrium shear modulus
G_∞	Infinite-frequency shear modulus

H	Enthalpy
k	Generic elastic constant
k_B	Boltzmann constant
l, l_y	Local strain and yield local strain, respectively
L	Length of one side of the (cubic) simulation box
m	Index of fragility or mass of a particle
M	Number of monomers per chain
N	Total number of particles (monomers) in the system
p, p_c	Degree of connectivity and percolation point, respectively
P	Pressure
$\mathbf{q}$	Wavevector used for representing the reciprocal lattice
$\mathbf{r}$	Position vector
r_c	Cut-off radius
r_{ij}	Distance between two particles
$\langle r \rangle$	Mean coordination number of the particles
R_{EE}	End-to-end distance along a polymer chain
R_G	Radius of gyration of a polymer chain or a generic cluster
S, S_C	Entropy and configurational entropy, respectively
$S(\mathbf{q})$	Structure factor
t	Time
t_w	Waiting time (*e.g.* time elapsed since a quench or a deformation)

T	Temperature
T_0	Critical temperature from VFT equation (see VFT below)
T_C	Critical temperature proposed by R.H. Colby (see Eq. (2.17))
T_G	Glass transition temperature
T_K	Kauzmann Temperature
T_{MC}	Critical temperature obtained from mode-coupling theory
T_R	Rigidity transition temperature
U	Potential energy
$\mathbf{v}$	Velocity
V	Volume
$W_i(t)$	Gaussian white-noise source

Note: Bold symbols denote vectorial form. These symbols are also used without a bold typeface to denote their moduli.

B.2 List of Greek letter symbols

$\alpha_2(t)$	Non-Gaussian parameter
Γ	Friction constant used in "Langevin MD"-based algorithm
ϵ	Strain, can also be used with two indexes corresponding to the plane along which the strain is applied
$\dot{\epsilon}_{\alpha\beta}$	Rate of strain
ε_{LJ}	Characteristic Lennard-Jones energy (sets the energy scale in the simulations)
ϕ	Fraction of mobile particles
Φ	Packing fraction
η	Zero shear-rate viscosity
μ	Shear modulus
ω	Frequency
σ	Radius of each particle (sets the length scale in the simulations)
$\sigma_{\alpha\beta}$	Element of the stress tensor, where the indexes α and β correspond to any two directions
τ, τ_α	General and alpha-relaxation times, respectively
χ	Temperature-rescaling factor used in the canonical ensemble
ξ	Correlation length

B.3 List of Acronyms

CPU	Central Processing Unit
FENE	Finitely Extensible Nonlinear Elastic
GK	Green-Kubo
GT	Glass Transition
LJ	Lennard-Jones
KWW	Kohlrausch-Williams-Watts (see Eq. (3.10)
MCT	Mode-coupling theory
MD	Molecular dynamics
MSD	Mean-square displacement
NGP	Non-Gaussian parameter
NPT	Isothermal-isobaric ensemble
NVE	Constant energy or microcanonical ensemble
NVT	Isothermal ensemble at constant volume (canonical ensemble)
PBC	Periodic boundary conditions
PE	Polyethylene
RDF	Radial distribution function
RT	Rigidity Transition
VFT	Vogel-Fulcher-Tammann (see Eq. (2.14))

Bibliography

[1] *Rigidity Theory and Applications*, edited by M.F. Thorpe and P.M. Duxbury (Plenum, New York, 1999).

[2] A.J. Rader, B.M. Hespenheide, L.A. Kuhn and M.F. Thorpe, Proc. Nat. Acad. Sci. U.S.A. **99**, 3540 (2002).

[3] M.F. Thorpe, D.J. Jacobs, M.V. Chubynsky and J.C. Phillips, J. Non-Cryst. Solids **266-269**, 859 (2000).

[4] A. Huerta and G.G. Naumis, Phys. Rev. B **66**, 184204 (2002); A. Huerta and G.G. Naumis, Phys. Rev. Lett. **90**, 145701 (2003); A. Huerta and G.G. Naumis, J. Non-Cryst. Solids **329**, 100 (2003).

[5] M. D. Ediger, C.A. Angell, and S. R. Nagel, J. Phys. Chem. **100**, 13200 (1996).

[6] C.A. Angell et al., J. Appl. Phys. **88**, 3113 (2000).

[7] P.A. Debenedetti and F.H. Sillinger, Nature **410**, 259 (2001).

[8] M. L. Wallace, B. Joós and M. Plischke, Phys. Rev. E **70**, 041501 (2004).

[9] G. Strobl, *The Physics of Polymers* (Springer-Verlag, Berlin, 1996).

[10] M. Plischke and B. Joós, Phys. Rev. Lett. **80**, 4907 (1998).

[11] B. Joós, M. Plischke, D.C. Vernon and Z. Zhou, in *Rigidity Theory and Applications*, edited by M.F. Thorpe and P.M. Duxbury (Plenum, New York, 1999) pp. 315-328.

[12] O. Farago and Y. Kantor, Europhys. Lett. **57**, 458 (2002).

[13] M.F. Thorpe, D.J. Jacobs, N.V. Chubynsky and A.J. Rader, in *Rigidity Theory and Applications*, edited by M.F. Thorpe and P.M. Duxbury (Plenum, New York, 1999) pp. 239-276.

[14] M.F. Thorpe, J. Non-Crust. Solids **57**, 355 (1983).

[15] X. Feng, W.J. Bresser and P. Boolchand, Phys. Rev. Lett. **78**, 4422 (1997).

[16] P. Boolchand, X. Feng, D. Selvanathan and W.J. Bresser in *Rigidity Theory and Applications*, edited by M.F. Thorpe and P.M. Duxbury (Plenum, New York, 1999) pp. 279-295.

[17] V. Trappe, V. Prasad, L. Cipelletti, P.N. Segre and D.A. Weitz, Nature **411**, 772 (2001).

[18] L. Cipeletti and L. Ramos, Curr. Opin. Colloid Interface Sci. **7**, 228 (2002).

[19] M. Adam and D. Lairez, *The Physical Properties of Polymeric Gels*, J.P. Cohen Addad, ed. (John Wiley and Sons, Ltd., New York, 1996).

[20] M. Plischke, D.C. Vernon, B. Joós and Z. Zhou, Phys. Rev. E **60**, 3129 (1999).

[21] D.C. Vernon, M. Plischke and B. Joós, Phys. Rev. E **64**, 031505 (2001).

[22] D. Staufer and A. Aharaony, *Introduction to Percolation Theory* (Taylor and Francis, London, 1994).

[23] K. Kremer and G.S. Grest, J. Chem. Phys. **92**, 5057 (1990).

[24] M. Doi and S.F. Edwards, *The Theory of Polymer Dynamics* (Clarendon, Oxford, 1986).

[25] C. Bennemann, J. Baschnagel, W. Paul, and K.Binder, Comput. Theor. Polym. Sci. **9**, 217 (1999); J. Baschnagel, C. Bennemann, W. Paul, and K. Binder, J. Phys.: Condens. Matter **12**, 6365 (2000).

[26] J. Buchholz, W. Paul, F. Varnik, and K. Binder, J. Chem. Phys. **117**, 7364 (2002).

[27] M.P. Allen and D.J. Tildesley, *Computer Simulations of Liquids* (Oxford University Press, New York, 1987).

[28] K. J. Rao, *Structural Chemistry of Glasses* (Elsevier, Oxford, 2002).

[29] K. Binder, J. Baschnagel, and W. Paul, Prog. Polym. Sci. **28**, 115 (2003).

[30] R.H. Colby, Phys. Rev. E **61**, 1783 (2000).

[31] W. Götze and L. Sjögren, Rep. Prog. Phys. **55**, 241 (1992).

[32] J. P. Hansen and I. R. McDonald, *Simple Theory of Liquids* (Academic, London, 1986).

[33] J. Perez, *Physique et Mécanique des Polymères Amorphes* (Technique et Documentation Lavoisier, Paris, 1992).

[34] G. Adam and J.H. Gibbs, J. Chem. Phys. **43**, 139 (1965).

[35] N. Giovambattista, S.V. Buldyrev, F.W. Starr and H.E. Stanley, Phys. Rev. Lett. **90**, 085506 (2003).

[36] P.K. Gupta in *Rigidity Theory and Applications*, edited by M.F. Thorpe and P.M. Duxbury (Plenum, New York, 1999) pp. 173-238.

[37] K. Okun, M. Wolfgardt, J. Baschnagel, and K Binder, Macromolecules **30**, 3075 (1997); C. Bennemann, J. Baschnagel and W. Paul, Eur. Phys. J. B **10**, 323 (1998); M. Aichele and J. Baschnagel, Eur. Phys. J. E **229**, 245 (2001).

[38] C. Bennemann, W. Paul, K. Binder, and B. Dünweg, Phys. Rev. E **57**, 843 (1998).

[39] C. Bennemann, W. Paul, J. Baschnagel, and K. Binder, J. Phys.: Condens. Matter **11**, 2179 (1999).

[40] C.A. Angell, in *Rigidity Theory and Applications*, edited by M.F. Thorpe and P.M. Duxbury (Plenum, New York, 1999) pp. 297-314.

[41] A.J. Liu and S.R. Nagel, Nature **396**, 21 (1998).

[42] M.E. Cates, J.P. Wittmer, J.-P. Bouchaud and P. Claudin, Phys. Rev. Lett. **81**, 1841 (1998).

[43] H. Tanaka, J. Meunier and D. Bonn, Phys. Rev. E **69**, 031414 (2004).

[44] J. Kurchan, C.R. Acad. Sci. (Paris) **2**, 239 (2001).

[45] W. Kob and J.-L. Barrat, Phys. Rev. Lett. **78**, 4587 (1997).

[46] W. Kob and J.-L. Barrat, Eur. Phys. J. B **13**, 319 (2000).

[47] J.-P. Bouchaud in *Soft and Fragile Matter: Nonequilibrium dynamics, Metastability and Flow*, edited by M. E. Cates and M. R. Evans (IOP Publishing, Bristol, 2000) pp. 285-304.

[48] J.-L. Barrat, J. Phys.: Cond. Mat. **15** S1 (2003).

[49] J.-P. Bouchaud, J. Physique **2**, 1705 (1992).

[50] P.Sollich, F. Lequeux, P. Hébraud and M.E. Cates, Phys. Rev. Lett. **78**, 2020 (1997).

[51] V. Viasnoff and F. Lequeux, Phys. Rev. Lett **89**, 065701 (2002); V. Viasnoff, S. Jurine and F. Lequeux, Faraday Discussions **123**, 253 (2003).

[52] W. Kob., C. Donati, S.J. Plimpton, P.H. Poole and S.C. Glotzer, Phys. Rev. Lett. **79**, 2827 (1997).

[53] R. Yamamoto and A. Onuki, Phys. Rev. E. **58**, 3515 (1998); R. Yamamoto and A. Onuki, Phys. Rev. Lett. **81**, 4915 (1998).

[54] M. Aichele, Y. Gebremichael, F.W. Starr, J. Baschnagel and S.C. Glotzer, J. Chem. Phys. **2003**, 5290 (2003).

[55] K. Vollmayr-Lee, W. Kob, K. Binder and A. Zippelius, J. Chem. Phys. **116**, 5158 (2002).

[56] C. Donati, J.F. Douglas, W. Kob, S.J. Plimpton, P.H. Poole and S.C. Glotzer, Phys. Rev. Lett. **80**, 2338 (1998).

[57] C. Bennemann, C. Donati, J. Baschnagel and S.C. Glotzer, Nature **399**, 246 (1999); Y. Gebremichael, T.B. Schrøder, F.W. Starr and S.C. Glotzer, Phys. Rev. E **64**, 051503 (2001);

[58] D. Long and F. Lequeux, Eur. Phys. J. E 4, 371 (2001); Y. Yilmaz, A. Erzan and Ö. Pekcan, Eur. Phys. J. E **9**, 135 (2002).

[59] C.T. Thurau and M.D. Ediger, J. Polym. Sci. Part B: Polym. Phys. **40**, 2463 (2002); C.T. Thurau and M.D. Ediger, J. Chem. Phys. **116**, 9089 (2002).

[60] M. Kröger and S. Hess, Phys. Rev. Lett **85**, 1128 (2000).

[61] S. Barsky, private communication.

[62] B. Joós and Z. Zhou, Phys. Rev. E **61**, 2410 (2000).

[63] D. Frenkel and B. Smit, *Understanding Molecular Simulation: From Algorithms to Applications* (Academic Press, San Diego, 2002).

[64] J. Felicity, M. Lodge and D.M. Heyes, J. Chem. Soc., Faraday Trans., **93**, 437 (1997).

[65] J.F.M. Lodge and D.M. Heyes, J. Chem. Soc., Faraday Trans. **93**, 437 (1997).

[66] J.F.M. Lodge and D.M. Heyes, Phys. Chem. Chem. Phys. **1**, 2119 (1999).

[67] F. Varnik and K. Binder, J. Chem. Phys. **117**, 6336 (2002).

[68] M.M. Hurley and P. Harrowell, Phys. Rev. E **52**, 1694 (1995).

[69] E.R. Weeks and D.A. Weitz, Phys. Rev. Lett **89**, 095704 (2002).

[70] C.A. Angell, P.H. Poole and J. Shao, Il Nuovo Cimento **16D**, 993 (1994).

[71] L.-S. Luo and G.D.J. Phillies, J. Chem. Phys. **105**, 598 (1996).

[72] E.R. Weeks, J.C. Crocker, A.C. Levitt, A. Schofield and D.A. Weitz, Science **287**, 627 (2000).

[73] J.C. Phillips, J. Non-Cryst. Solids **34**, 153 (1979).

[74] G.G. Naumis, Phys. Rev. B **61**, R9205 (2000).

[75] A. Huerta and G.G. Naumis, Phys. Lett. A **299**, 660 (2002).

[76] A.M. Puertas, M. Fuchs and M.E. Cates, Phys. Rev. Lett **88**, 098301 (2002).

[77] S.J. Barsky and M. Plischke, Phys. Rev. E **53**, 871 (1996).